

An expanded database of Southern Hemisphere surface sediment dinoflagellate cyst assemblages and their oceanographic affinities

Lena M. Thöle¹, Peter D. Nooteboom^{2,3}, Suning Hou¹, Rujian Wang⁴, Senyan Nie⁴, Elisabeth Michel⁵, Isabel Sauermilch¹, Fabienne Marret⁶, Francesca Sangiorgi¹, Peter K. Bijl¹

¹Department of Earth Sciences, Utrecht University, Utrecht, Netherlands.

²Institute for Marine and Atmospheric research Utrecht (IMAU), Department of Physics, Utrecht University, Utrecht, the Netherlands

³Centre for Complex Systems Studies, Utrecht University, Utrecht, the Netherlands

⁴State Key Laboratory of Marine Geology, Tongji University, Shanghai, China

⁵Laboratoire des Sciences du Climat et de l'Environnement, LSCE/IPSL, Universit. de Paris-Saclay, Gif sur Yvette, France

⁶Department of Geography and Planning, School of Environmental Sciences, University of Liverpool, United Kingdom

Correspondence to: P.K. Bijl (p.k.bijl@uu.nl) twitter handle: @peterbijlwilkes

This paper is a non-peer reviewed preprint submitted to EarthArXiv. The paper is has been resubmitted to Journal of Micropaleontology.

An expanded database of Southern Hemisphere surface sediment dinoflagellate cyst assemblages and their oceanographic affinities

Lena M. Thöle¹, Peter D. Nooteboom^{2,3}, Suning Hou¹, Rujian Wang⁴, Senyan Nie⁴, Elisabeth Michel⁵, Isabel Sauermilch¹, Fabienne Marret⁶, Francesca Sangiorgi¹, Peter K. Bijl¹

¹Department of Earth Sciences, Utrecht University, Utrecht, Netherlands.

²Institute for Marine and Atmospheric research Utrecht (IMAU), Department of Physics, Utrecht University, Utrecht, the Netherlands

³Centre for Complex Systems Studies, Utrecht University, Utrecht, the Netherlands

⁴State Key Laboratory of Marine Geology, Tongji University, Shanghai, China

⁵Laboratoire des Sciences du Climat et de l'Environnement, LSCE/IPSL, Université de Paris-Saclay, Gif sur Yvette, France

⁶Department of Geography and Planning, School of Environmental Sciences, University of Liverpool, United Kingdom

Correspondence to: P.K. Bijl (p.k.bijl@uu.nl)

Abstract. Dinoflagellate cyst assemblages present a valuable proxy to infer paleoceanographic conditions, yet factors influencing geographic distributions of species remain largely unknown, especially in the Southern Ocean. Strong lateral transport, sea-ice dynamics and a low and uneven geographic coverage of surface sediment samples have limited the use of dinocyst assemblages as a quantitative proxy for paleo-environmental conditions such as sea-surface temperature (SST), nutrient concentrations, salinity and sea ice (presence).

In this study we present a new set of surface sediment samples (n=66) from around Antarctica, doubling the number of Antarctic-proximal samples to 100 (dataset wsi_100) and increasing the total number of Southern Hemisphere samples to 655 (dataset sh_655). Additionally, we use modelled ocean conditions and apply Lagrangian techniques on all Southern Hemisphere sample stations to quantify and evaluate the influence of lateral transport on the sinking trajectory of microplankton and through that, to the inferred ocean conditions.

K-means cluster analysis on the wsi_100 dataset demonstrates the strong affinity of *Selenopemphix antarctica* to sea-ice cover conditions, and *Islandinium* spp. to low-salinity conditions. For the entire Southern Hemisphere, the *k*-means cluster analysis identifies nine clusters with a characteristic assemblage. In most clusters a single dinocyst species dominates the assemblage. These clusters correspond to well-defined oceanic conditions in specific Southern Ocean zones or along the ocean fronts. We find that when lateral transport is predominantly zonal, the environmental parameters inferred from the sea floor assemblages mostly correspond to those of overlying ocean surface. In this case, the transport factor can thus be neglected and will not represent a bias in the reconstructions. Yet, for some individual sites, e.g., deep water sites or sites under strong current regimes, lateral transport can play a large role. The results of our study further constrain environmental conditions represented by dinocyst assemblages and the location of Southern Ocean frontal systems.

1. Introduction

Dinoflagellate cyst assemblages have been increasingly used as a proxy to reconstruct southern high-latitude oceanographic conditions for the late Paleogene to recent (34–0 million years ago; Esper and Zonneveld, 2007; Prebble et al., 2016; Sangiorgi et al., 2018; Bijl et al., 2018a; Hoem et al., 2021a, b; Marschalek et al., 2021). Such reconstructions rely on an accurate understanding of the modern ecological affinities of taxa. For extant species, modern biogeography is statistically linked to surface oceanographic conditions (sea-surface temperature, nutrients, salinity, sea-ice; de Vernal et al., 2005; Zonneveld et al., 2013; Prebble et al., 2013; Mudie et al., 2017; Marret et al., 2020; see Table 1 for an overview). They all assume that the assemblages in a surface sediment sample at a certain location represent the parameters of (and derive from) the sea water directly above the sediment. Transfer function techniques then offer a quantitative approach to directly translate (down-core) assemblages into values of past environmental parameters (e.g., Marret et al., 2001; de Vernal et al., 2005; Esper and Zonneveld, 2007). This requires a sufficiently large training set, a good number and geographic spread of surface sediment samples, so that the full variety of surface oceanographic conditions is represented.

Constraining oceanographic affinities of dinocyst species has been hindered by the low number and uneven geographic distribution of surface sediment samples from the Southern Ocean, particularly when compared to that in the Northern Hemisphere high latitudes (de Vernal et al., 2001; 2020). Notably scarce are samples from the Antarctic margin, i.e., the region south of the Polar Front (Marret et al., 2020). Among the most dominant species found close to the Antarctic margin, with high environmental relevance is *Selenopemphix antarctica*, generally associated to (past) Southern Ocean sea-ice presence (Harland and Pudsey, 1999; Marret et al., 2001; Houben et al., 2013). Sporadic occurrences of *S. antarctica* north of the winter sea-ice edge (Esper and Zonneveld 2007) may be linked to northwards transport by surface and deep currents from the sea-ice zone (Nooteboom et al., 2019). Yet, the low number of samples so far analysed from close to the Antarctic margin makes the sea-ice affinity of *S. antarctica* poorly constrained. Specifically, it is unknown what the regional applicability of *S. antarctica* as a sea-ice indicator may be, and whether whole dinocyst assemblages from sea-ice regions may be more suitable than a single species to constrain past sea-ice conditions.

Previous attempts to apply transfer functions with surface sediment samples from the Southern Ocean focused on sea-surface temperature (SST) reconstructions (Marret et al., 2001; Esper and Zonneveld, 2007). Pleistocene dinocyst assemblages from the subtropical front in the Pacific Ocean yield realistic SST reconstructions for the interglacial time intervals in agreement with other proxies, but colder than those obtained with other proxies for glacial intervals (Marret et al., 2001). This is foremost due to the occurrence of *S. antarctica* in glacial phases, which results in a cold bias in the transfer function output (Prebble et al., 2016). The extensive surface sediment sample set from around New Zealand (Prebble et al., 2013) demonstrated that *S. antarctica* is a rare member of dinocyst assemblages in the subantarctic Pacific, and in that region its presence cannot be easily explained by lateral transport (Nooteboom et al., 2019). This leaves questions about the true sea-ice affinity of this species. Esper and Zonneveld (2007) showed overall good consistency in SST reconstructions based on dinocysts compared to that

65 from other proxies for sediment cores spanning the past 140 kyrs, with some potential bias due to selective degradation of dinocysts (Esper and Zonneveld, 2007).

Table 1. Dinocyst compilation efforts. DCA = Detrended correspondence analysis, CCA = Canonical Correspondence analysis, MAT = Modern Analogue Technique

Source	# samples	Statistical method
Marret et al., 2001	81 (Southern Hemisphere)	Multivariate analyses (non-metric multidimensional scaling—MDS), Best analogue method
Marret and Zonneveld, 2003	835 (global)	DCA, CCA – to explore which environmental variables explain dinocyst assemblages most
Esper and Zonneveld, 2007	138 (Southern Hemisphere)	CCA, MAT – – to explore environment controls on dinocyst distribution
Prebble et al., 2013	311 (Southern Hemisphere)	Cluster analyses (<i>k</i> -means clustering) – to explore environment controls on dinocyst distribution
Zonneveld et al., 2013	2405 (global)	-
Nooteboom et al., 2019	2405 (global)	Lagrangian particle trace simulations in ocean model to demonstrate the effect of lateral transport on dinocyst distributions
Marret et al., 2020	3636 (global) 595 (Southern Hemisphere)	-
This study	655 (Southern Hemisphere)	Cluster analyses (<i>k</i> -means clustering) – to explore environment controls on dinocyst distribution

70

Lateral transport of sinking particles creates a deviation in the first-order approximation that plankton (or other particles) found in the sediments relate to oceanographic conditions in the directly overlying surface waters (e.g., Zonneveld et al., 2013). For instance, Nooteboom et al. (2019) showed that at realistic assumptions on sinking speed of pelagic particles in their descent towards the ocean floor, lateral transport can affect the location of deposition. The effect of lateral transport on sinking particles is large in places with deep (>1 km) waters and strong currents, in locations where currents flow meridionally (because that is the main direction of environmental gradients), but also where turbulence occurs during sinking (Nooteboom et al., 2019).

75

Taking lateral transport into account could help to understand whether sedimentary plankton assemblages found at a certain location relate to the directly overlying surface oceanographic conditions at the same location.

In this study, we present dinocyst assemblage data from a new surface sediment sample set predominantly from the Antarctic margin. This sample set fills a clear gap in previously underrepresented ice-proximal Southern Hemisphere surface sediment samples. Moreover, the wide geographic spread of these new samples allows investigation of longitudinal differences in ice-proximal dinocyst assemblages.

Adding these to existing surface sediment samples of the Southern Hemisphere allows an improved assessment of biogeographic and oceanographic affinities of Southern Hemisphere dinocyst assemblages. We compare dinocyst assemblages to the following oceanographic parameters: SST, salinity, nutrients (nitrate and silicate concentrations), and sea ice cover. We assess these by analysing model output data, specifically for the surface water directly overlying the sites, and for the surface water in the location of origin of simulated particles that descended to those sites. This allows an evaluation to what extent lateral transport affects the paleoceanographic affinities of sedimentary dinocyst assemblages.

2. Modern oceanographic conditions

2.1 The Southern Ocean

The dominant oceanographic feature in the Southern Ocean is the Antarctic Circumpolar Current (ACC; Marshall and Speer, 2012). Without land barriers and (partly) driven by strong Southern Hemisphere Westerly Winds, the ACC runs clockwise around Antarctica and is the world's strongest ocean current with 140 Sv (Orsi et al., 1995, Park et al., 2019 and reference therein) or higher. At ACC-associated ocean fronts, the flow speed is the highest, which introduces strong environmental gradients and create quasi-latitudinal zones with characteristic environmental conditions (Fig. 1; Orsi et al., 1995). From north to south, the main fronts are the Subtropical Front (STF), the Subantarctic Front (SAF), and the Polar Front (PF; Fig. 1).

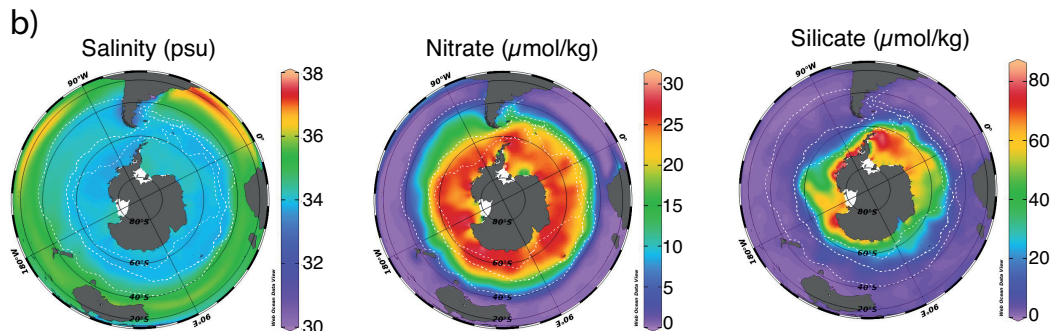
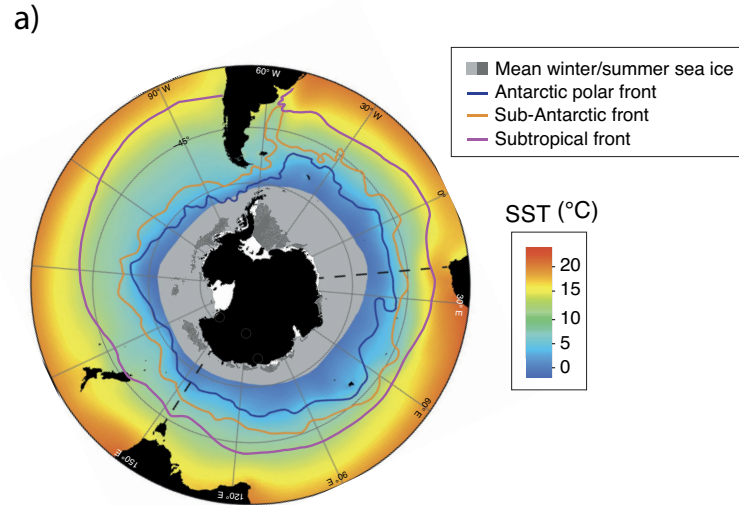
In general, the STF is considered the northern boundary of the ACC (Orsi et al., 1995). On a 0.5° latitudinal band, it introduces a surface temperature and salinity change of 4–5°C and ~0.5 respectively, separating warm and nutrient-poor Subtropical Surface Waters of the subtropical gyres north of it from colder and nutrient-rich Subantarctic Surface Waters of the Subantarctic Zone (SAZ; see Fig. 1).

The SAF separates the SAZ from the Polar Frontal Zone (PFZ), in which Subantarctic Surface Waters are subducted and form Antarctic Intermediate Waters (Orsi et al., 1995). The PF separates these waters from colder (<2°C) Antarctic Surface Waters that form the Antarctic Zone (AZ). The typical high-nutrient-low-productivity-signature (HNLP) of the AZ is caused by a scarcity of light and micro-nutrients limiting the utilization of available macro-nutrients. Overall, this leads to a dominance of silicate-based phytoplankton (e.g., diatoms) over calcareous species (e.g., coccolithophores). Excess nutrients that are depleted in silicate compared to calcium can diffuse into other zones and fuel productivity there.

In the AZ, (seasonal) sea ice plays a major role as it can strongly modulate light and nutrient availability (Mitchell et al., 1991). Sea ice is mostly focused on areas close to the Antarctic continent, the Ross and Weddell Seas, and Prydz Bay, where brine

110 rejection promotes the formation of Antarctic Bottom Water, sinking to the ocean abyss (Adkins, 2013; Talley, 2013, Solodoch et al., 2022).

However, different sea-ice dynamics prevail in the Ross and Weddell Seas. The Weddell Sea has a strong, dynamic gyre that is transporting the formed sea ice and icebergs out of the Weddell Sea into the South Atlantic, known as Iceberg Alley (Orsi et al., 1995). The most prominent feature in the Ross Sea is the Ross Sea polynya, open patches in the sea ice, maintained by katabatic winds (Rhodes et al., 2009; Bromwich et al., 1992).



115

Figure 1: Compilation of maps of modern environmental parameters in the Southern Ocean. a) Southern Ocean SST and approximate winter and summer sea ice extent (modified from Crosta et al., 2021 and Spreen et al., 2015–2021). b) Surface (1 meter) salinity (psu), nitrate and silicate concentrations ($\mu\text{mol/kg}$). Data from the World Ocean Atlas (Locarnini et al., 2018).

2.2 Lateral transport

120 Taking (past) lateral transport into account in the interpretation of sediment proxies remains difficult, as the quantification of transport comes with large uncertainties and assumptions regarding (past) ocean current strengths and directions, particle aggregation and size and – connected to this – their sinking speed (Nooteboom et al., 2019). Recent efforts have attempted to

better constrain the influence of lateral transport in sedimentary microplankton assemblages by applying Lagrangian particle trace experiments in ocean model simulations with a spatial resolution high enough to represent an eddying flow (0.25° and finer; Nooteboom et al., 2019). In the Southern Ocean especially, it is thought that the ACC strength and sea-ice dynamics can assert a large influence on particle transport. Here, recent modelling efforts could explain unexpected, rare occurrences of species (Nooteboom et al., 2019) outside their common habitat. More specifically, findings of *Selenopemphix antarctica* north of the SAF could be attributed to latitudinal transport from the AZ, thus helping to better constrain and interpret (past) ecological affinities of single species and explain their rare presence in unexpected locations. This demonstrated the potential influence lateral transport may play in shaping microplankton assemblages, and, through that, the inferred surface oceanographic affinities of microplankton species.

3. Methods

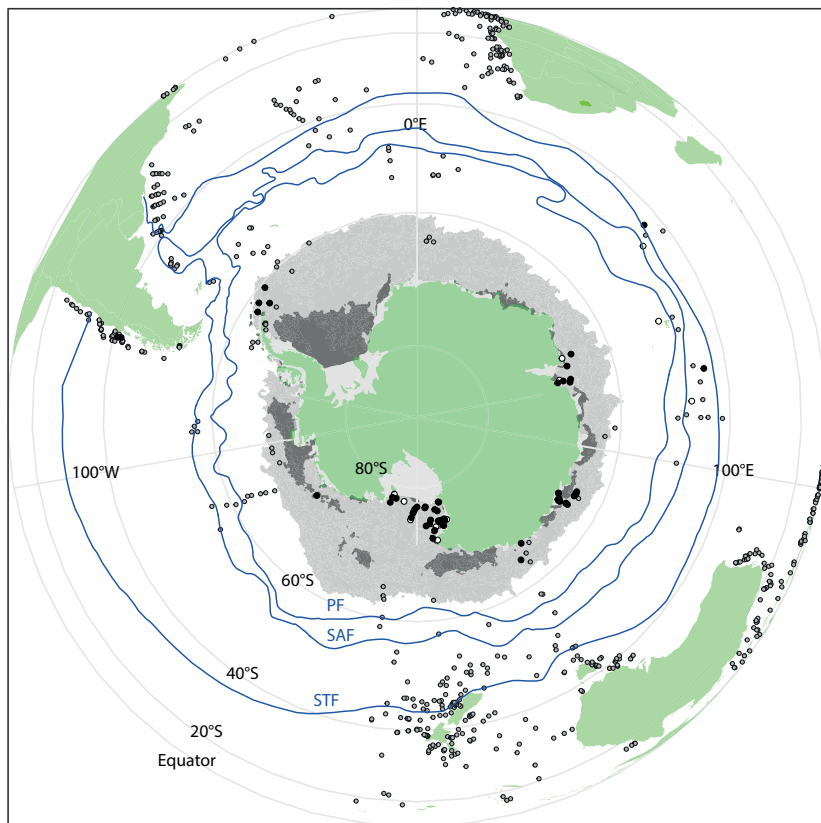
3.1 New surface sediment samples from around Antarctica

In total, 66 new surface sediment samples located close to the Antarctic continent and 7 samples located north of the modern Polar Front were collected (Fig. 2; Table 2) during various cruises. For some new samples, existing age models confirmed a modern or (late?) Holocene age (e.g., Hartman et al., 2018; Wilson et al., 2018; Armand et al., 2018; Behrens et al., 2019). For many samples, however, no absolute age determination was available, but the use of box coring technique (Table 1) for retrieving the sediment-water interface and the dinocyst assemblages and palynofacies found (e.g., presence of more labile organic matter, such as amorphous organic matter and chitin remains) suggest a tentative modern-to-late Holocene age. Previous studies on modern surface sediments used an age-cut off at 7 ka (Prebble et al., 2013). We are confident that the data added here have a similarly modern age as the data we compare ours to. It does mean that the current surface sediment sample set averages out potential environmental changes that occurred in the Holocene.

All samples, but particularly those from the Antarctic continental margin, may have contributions of reworked palynomorphs from older sediments (Bijl et al., 2018b). Most reworking is easily recognized (and excluded from further analysis) because they are extinct. For extant taxa, such as *Spiniferites ramosus*, *Operculodinium centrocarpum*, *Nematosphaeropsis labyrinthus*, it is impossible to assess from their appearance whether they are reworked or in situ. This means that caution should be taken when interpreting rare occurrences of taxa.

A total of 46 productive samples are south of 60°S, located in the Ross Sea (28 samples), the Sabrina coast (17 samples), Prydz Bay (6 samples) and Weddell Sea (4 samples), almost doubling the number of existing samples from Antarctic ice-proximal sites to 100. We add the first dinocyst assemblages south of 70°S (Ross Sea, Fig. 2), yet some ice-proximal areas remain uncovered, such as the Weddell Sea or offshore Dronning Maud Land as well as most of the West Antarctic continental margin. The seven additional samples are located close to Crozet Island, on the Kerguelen Plateau and along the west coast of the South America (Fig. 2).

Most samples are in (relatively) close proximity to land, close to the coast of New Zealand, the western coasts of Southern
155 Africa and Australia and both sides of South America. The Atlantic depicts the highest spatial coverage, whereas the Pacific
and Indian Ocean appear underrepresented.



160 **Figure 2: Overview map of all available surface sediment data for the Southern Hemisphere. Grey dots with black outlines represent samples that have been previously published (Marret et al., 2020), black dots are newly counted samples from this study, while dots with black outline represent new samples that did not yield enough dinocysts to be included in further analyses. Also plotted are ACC frontal systems (blue lines, STF = Subtropical Front, SAF = Subantarctic Front, PF = Polar Front). Winter and Summer sea ice derived from Spreen et al. (2015–2021).**

Table 2. List of newly counted samples

Station	Sample method	Latitude	Longitude	Adjusted Latitude in ocean model	Adjusted Longitude in ocean model	Water depth (m)	in SH_655	in WSI_100
ANT 33_RS78	Box core	-78.6939	-163.6669	NA	NA		n	n
ANT 33_A1-08	Box core	-78.1719	-165.7881	-76.9000	-165.7881	498	y	y
ANT 33_A1-07	Box core	-78.1681	-163.0389	-76.9000	-163.0389	679	y	y
ANT 33_A1-10	Box core	-77.9681	-171.3731	NA	NA		n	n
ANT 33_A1-20	Box core	-77.6661	165.8850	-76.9000	165.8850	590	y	y
ANT 31_JB01	Box core	-77.5883	165.5694	-76.9000	165.5694	774	y	y
ANT 33_A1-05	Box core	-77.3961	-162.6781	-76.9000	-162.6781	658	y	y
ANT 32_RB08B	Box core	-77.3089	179.8525	-76.9000	179.8525	670	y	y
ANT 32_RB11B	Box core	-77.2694	174.5997	-76.9000	174.5997	494	y	y
ANT 33_A1-15	Box core	-77.1269	174.9639	-76.9000	174.9639	400	y	y
ANT 32_RB07B	Box core	-77.0497	-178.9003	-76.9000	-178.9003	628	y	y
ANT 32_RB06B	Box core	-76.7133	-178.2403			619	y	y
BC22	Box core	-76.6930	169.0780			800	y	y
ANT 33_A1-18	Box core	-76.4211	167.7239			743	y	y
ANT 32_RB05B	Box core	-76.4053	-177.7194			606	y	y
ANT 32_RB03B	Box core	-75.7467	-176.8697			610	y	y
ANT 32_RB02B	Box core	-75.4233	-176.4858				n	n
ANT 31_JB04	Box core	-75.3011	172.3725			511	y	y
ANT 33_I5	Box core	-75.0869	165.0481			1174	y	y
ANT 31_R09	Box core	-75.0033	165.9980			1032	y	y
ANT 31_R08	Box core	-75.0030	165.0120				n	n
ANT 31_R10	Box core	-75.0022	167.0019			636	y	y
ANT 35_R1-03	Box core	-74.9953	168.3578			349	y	y
ANT 31_R11	Box core	-74.9492	167.8056			449	y	y
ANT 31_R14	Box core	-74.9350	164.8047			901	y	y

ANT 31_R18	Box core	-74.9130	163.7650				n	n
ANT 31_R02	Box core	-74.7850	165.1330	-74.8022	165.1150	719	y	y
ANT 31_R05	Box core	-74.7767	167.7775			586	y	y
ANT 31_JB05	Box core	-74.7553	173.1881			497	y	y
ANT 32_RB16B	Box core	-74.5136	175.1217			478	y	y
ANT 33_A2-02	Box core	-74.2061	170.1181				n	n
ANTA02_AV43	Box core	-74.1410	166.0830	-74.1325	166.1983		y	y
ANT 33_A2-03	Box core	-73.7011	170.9789			588	y	y
ANT 33_A2-05	Box core	-72.6050	172.4369			546	y	y
ANT 31_R19	Box core	-72.2544	170.3944				n	n
ANT 32_AB18B	Box core	-71.8986	-128.1450			3463	y	y
ANT 30_IS-01	Box core	-69.2594	76.3775			260	y	y
ANT 29_P6-12	Box core	-68.9095	75.4897				n	n
ANT 29_P7-16	Box core	-68.3836	76.1972			558	y	y
ANT 29_P3-09	Box core	-67.5123	68.0119				n	n
ANT 29_P7-14	Box core	-67.4378	77.1840			311	y	y
ANT 29_PA-05	Box core	-67.2357	76.1799			353	y	y
ANT 29_PA-01	Box core	-67.2061	71.2824			487	y	y
NBP1402_KC13	Kasten core	-66.8730	118.2400			646	y	y
NBP1402_KC14	Kasten core	-66.8730	118.2370			643	y	y
NBP1402_KC42	Kasten core	-66.4840	120.3320			610	y	y
U1357B	Piston core	-66.4133	140.4262			1017	y	y
NBP1402_KC9	Kasten core	-66.3610	119.8620			683	y	y

NBP1402_SMG51	Kasten core	-66.3240	120.4650			450	y	y
NBP1402_27A	Kasten core	-66.1850	120.5040			544	y	y
NBP1402_KC27B	Kasten core	-66.1850	120.5040			547	y	y
NBP1402_JKC53	Kasten core	-66.1840	120.5030			545	y	y
NBP1402_MC_45	Multicore	-66.1830	120.5010			537	y	y
NBP1402_KC57	Kasten core	-66.1289	120.4640				n	n
ANT 29_P3-03	Box core	-66.0000	67.8115			2689	y	y
SABRINA_KC11	Kasten core	-65.1320	120.0490			2611	y	y
SABRINA_PC7	Piston core	-65.1310	120.0490			2611	y	y
SABRINA_PC6	Piston core	-64.8190	120.1430			3012	y	y
SABRINA_KC14	Kasten core	-64.5390	116.6400			2100	y	y
SABRINA_KC2	Kasten core	-64.4710	115.6230			2161	y	y
SABRINA_KC3	Kasten core	-64.4630	115.0430			1862	y	y
U1361A	Piston core	-64.4100	143.8900			3454	y	y
ANT 30_D2-10	Box core	-62.9600	-52.2667			974	y	y
ANT 30_D1-07	Box core	-62.2428	-56.5769			3548	y	y

ANT 30_D2-05	Box core	-61.5850	-54.1500			450	y	y
ANT 30_DA-02	Box core	-60.8350	-49.5817			2592	y	y
MD11-3352CQ	Box core	-50.5672	68.3858				n	n
MD12-3396CQ	Box core	-47.7313	86.6952				n	n
MD04-2716CQ	Box core	-46.1650	52.9267				n	n
MD12-3401CQ	Box core	-44.6788	80.3930			3445	y	n
MD04-2714CQ	Box core	-43.3983	49.8200			2300	y	n
MD07-3100	Calypso	-41.6022	-74.9567			1609	y	n
MD07-3098	Calypso	-40.9300	-75.0303			3055	y	n

165 3.2 Palynology

Samples were processed for palynological analysis following standard procedures of the Laboratory of Paleobotany and Palynology (e.g., Bijl et al., 2018b). Sediment samples were freeze-dried, crushed, and weighed, before a tablet (# 19855) of known amount of *Lycopodium clavatum* was added to quantify dinoflagellate cyst concentrations. Samples were then treated with 30% hydrochloride acid (HCl) and 38% cold hydrofluoric acid to respectively dissolve carbonates and silicates. A second round of 30% HCl treatment removed fluoric gels that might have formed, before the acid-sample mix was centrifuged and decanted. The (organic) residue was sieved at 250 and 10 µm and an ultrasonic bath assisted to disaggregate organic particles. The residue was mounted on glass slides in glycerin jelly. Dinoflagellate cysts were then counted under light-transmitted microscope.

Where possible, specimens were identified to species level at 400x magnification. Taxonomy followed that cited in Williams et al. (2017), and informal taxonomic descriptions in Esper and Zonneveld (2007) for some subspeciation. To facilitate the integration of our analyses with previously published data sets (Prebble et al., 2013; Marret et al., 2020), we grouped different dinocyst species the same way. This led to the following taxonomic grouping:

1. *Brigantedinium* spp.: *Brigantedinium cariacense*, *Brigantedinium simplex*, and *Dubridinium capitatum*
2. *Protoperidiniacean* cysts: *Lejeunecysta* spp., cysts of *Protoperidinium stellatum*, *Quinquecuspis concreta*, and *Votadinium calvum*
3. *Nematosphaeropsis labyrinthus*: all *Nematosphaeropsis* species
4. *Spiniferites hyperacanthus* was combined with *Spiniferites mirabilis*
5. *Spiniferites bulloides* was combined with *Spiniferites ramosus*
6. *Spiniferites belerius* was combined with *Spiniferites membranaceus*
7. Cysts of *Protoperidinium nudum* were assigned to *Selenopemphix quanta*

8. All *Echinidinium* species were grouped
9. Cysts of *Polarella glacialis* were counted but not included in the dinocyst sum
10. *Selenopemphix* sp. 1 (Esper and Zonneveld, 2007) was counted separately from *Selenopemphix antarctica*, but these were grouped in the cluster analyses of wsi_100 and sh_655.
- 190 11. *Gymnodinium* spp.: all species of *Gymnodinium*

In general, up to 100 (200 when possible) cysts (excluding *Polarella*) were counted per sample. This number captured the full diversity in our samples (see Fig. S1 for rarefaction analysis). As minimal cutoff, 13 samples with total counts < 25 were excluded from further analyses. In this paper, we describe dinocyst abundances categorically as follows: rare = >1% of assemblage, few = 1–10%, common = 10–25%, abundant = 25–50%, dominant = >50%.

We excluded the cysts of *Polarella glacialis* in further data analyses for the following reasons: (1) ambiguity about whether the absence of *Polarella* in other studies is the result of its real absence or is due to other reasons. For instance, a coarser than 10 microns mesh size often used for sieving samples could result in the loss of *Polarella* due to its small size. This obscures presentation of biogeographic patterns for this species (2) the short stratigraphic range of the species (few hundred years, both in samples from the Ross Sea and from Wilkes Land; Sangiorgi, pers. obs., and Hartman pers. comm., respectively) in the cores analyzed so far could imply that its presence in the sediment is linked to preservation exclusively in relatively freshly deposited samples. It remains possible that *Polarella* abundance can be used as indicator for sea ice if they were found in older sediments. With the existing knowledge, the potential of *Polarella* in paleoreconstructions is yet very limited. (3) its overwhelming abundance in many modern samples, which dilutes the taxa that do occur further down in the stratigraphic record. Since this study is intended to improve dinocyst assemblage-based tools for paleoreconstructions, adding a modern cyst species that has no stratigraphic record does not help. The *Polarella* counts are available in the dataset on Github (Bijl, 2022), but not included in relative abundance calculations for the rest of this paper.

3.3 Data sets

To evaluate regional biogeographic consistency in ice-proximal assemblages, we created a data subset containing only sample locations with sea ice in the overlying waters. For this, we used modern modeling data and the criterion of Antarctic winter (June, July, August; JJA) sea-ice presence > 0 (see section 3.5 below). This sub-dataset (“wsi_100”) contains 100 samples. We then added all new samples (Table 2) to the Southern Hemisphere samples of the latest existing global compilation of dinocyst surface sediments (Marret et al., 2020). This yields 655 samples in total (dataset “sh_655”).

Data of this paper is stored at Github (Bijl, 2022). The environmental data corresponding to locations of wsi_100 and sh_655 are obtained from the Nucleus for European Modelling of the Ocean (NEMO; Madec, 2016) ocean model, which is coupled to the MEDUSA-2.0 biogeochemical model (Yool et al., 2013), Following the approach as detailed in Section 3.5.

3.4 Cluster Analyses

220 The clustering of surface samples allowed us to explore spatial relationships between dinocyst assemblages and surface oceanographic conditions. These relationships in the modern day can be used to infer paleoceanographic conditions from fossil assemblages. Following the method of Prebble et al. (2013), we performed *k*-means cluster analyses on the relative abundance of dinocyst species for the two data sets. We ran 100 replications for each cluster solution and chose the most stable clustering. The evaluation of the clustering of wsi_100 and sh_655 can be found in Fig. S2 and S3. All analyses were done in R using the package dbSCAN (Hahsler et al., 2019).

3.5 Surface oceanographic parameters: surface versus transport data – particle tracking

225 To identify environmental conditions associated with the different clusters, we analysed SST (°C), sea-ice presence (from 0–1, fraction of grid cell that is sea ice-covered), salinity (psu), nitrate (mmol/m³) and silicate (mmol/m³) in the surface waters at the location of the surface sediments. For this, we made use of the ORCA0083-N06 output from the NEMO (Madec, 2016) ocean model, which is coupled to the MEDUSA-2.0 biogeochemical model (Yool et al., 2013). We note that the density of environmental observations at high latitudes is low, and as such the verification of the model output comes with an unknown
230 degree of uncertainty. To evaluate the impact of particle transport, we compared the conditions in the overlying surface water to those of modelled backtracked surface water locations. The NEMO model provides a global three-dimensional flow field with 5-daily output and has 1/12° horizontal resolution with 75 unevenly distributed vertical layers, properly reflecting the transport of Lagrangian particles by mesoscale and sub-mesoscale eddies (Nooteboom et al., 2020; Qin et al., 2014). In the first run, we recorded the surface water conditions of the overlying surface sediment locations, every three days from 2000-
235 01-03 until 2003-12-30. In the second run, we released virtual particles every three days for four years (from 2000-01-03 until 2003-12-30, using the OceanParcels Lagrangian Simulator, Lange and van Sebille, 2017; Delandmeter and van Sebille, 2019) at the sediment surface location and backtracked them to the ocean surface setting a 25 m day⁻¹ sinking speed. This sinking speed is faster than the sinking of individual dinoflagellate cysts, as we assume some degree of material aggregation (Nooteboom et al., 2019).

240 The southern boundary of the NEMO model set up was at 77 °S. As a result we had to relocate 11 samples that were originally located more southward to a latitude of 76.9 °S for the model run (Table 2), assuming minimal effects on environmental and transport conditions. Similarly, nine sample locations were too close to land and, due to the model resolution, appeared on land in the model. Thus, their location was adjusted (Table 2) to the nearest ocean site by minimally shifting the latitude and/or longitude.

4.1 New Southern Hemisphere surface samples

The 66 newly analyzed productive samples contain 24 different species (Fig. 3). Although we counted *Selenopemphix antarctica* and *Selenopemphix* sp. 1 (after Esper and Zonneveld, 2007) separately, the two species were not counted separately in previously published data sets (most of the data simply refer to *Selenopemphix antarctica*). In our cluster analysis, the two
250 species are hence combined as *Selenopemphix antarctica*. All new samples from Antarctic-proximal sites are dominated by heterotrophic peridinioid (P) cysts (Fig. 3). The most equatorward new samples (Fig. 3b, i) show abundant to dominant *Brigantedinium* spp., *Impagidinium* spp., *Nematosphaeropsis labyrinthus* and *Spiniferites* spp. Typical ice-proximal species *S. antarctica* and *Nucicla umbiliphora* (e.g., Hartman et al., 2018) are rare or absent.

In the samples from the Weddell Sea (Fig. 3b, ii), *Islandinium minutum* is dominant, with very low contributions from
255 *Selenopemphix antarctica*, *Brigantedinium* spp. or *Impagidinium pallidum*. The samples from Prydz Bay (Fig. 3b, iii) have a rather diverse assemblage with abundant *Selenopemphix antarctica* and common *Selenopemphix* sp.1, *Nucicla umbiliphora*, *Islandinium minutum* and *Brigantedinium* spp. In the sample further north and out of the Bay (ANT29_P3_03), *Impagidinium pallidum* dominates, with common *Operculodinium centrocarpum*. In the samples from Sabrina Coast (Fig. 3b, iv), *Selenopemphix antarctica* sp. 1 is abundant, with rare to few *Selenopemphix* sp.1, *Nucicla umbiliphora*, and *Islandinium*
260 *minutum*. A striking distinction can be made between the Sabrina and NBP samples, with the latter having abundant *Brigantedinium* spp. and the former having abundant *Impagidinium pallidum* (>30%), common *Operculodinium centrocarpum*, and few *Pyxidinoopsis reticulata* and *Spiniferites mirabilis*. Most of the Ross Sea samples contain a quite uniform assemblage (Fig. 3b, v), with dominant *Selenopemphix antarctica* sp. 2 and/or *Nucicla umbiliphora*. In most samples, one of the species is clearly dominant. *Selenopemphix antarctica*, *Islandinium minutum*, *Brigantedinium* spp. and
265 *Operculodinium centrocarpum* are rare. In one sample located outside of the Ross Sea (ANTA02_AV43), *Brigantedinium* spp. dominates, with common *Impagidinium pallidum* and *Selenopemphix antarctica*.

a) Map of new surface sediment samples

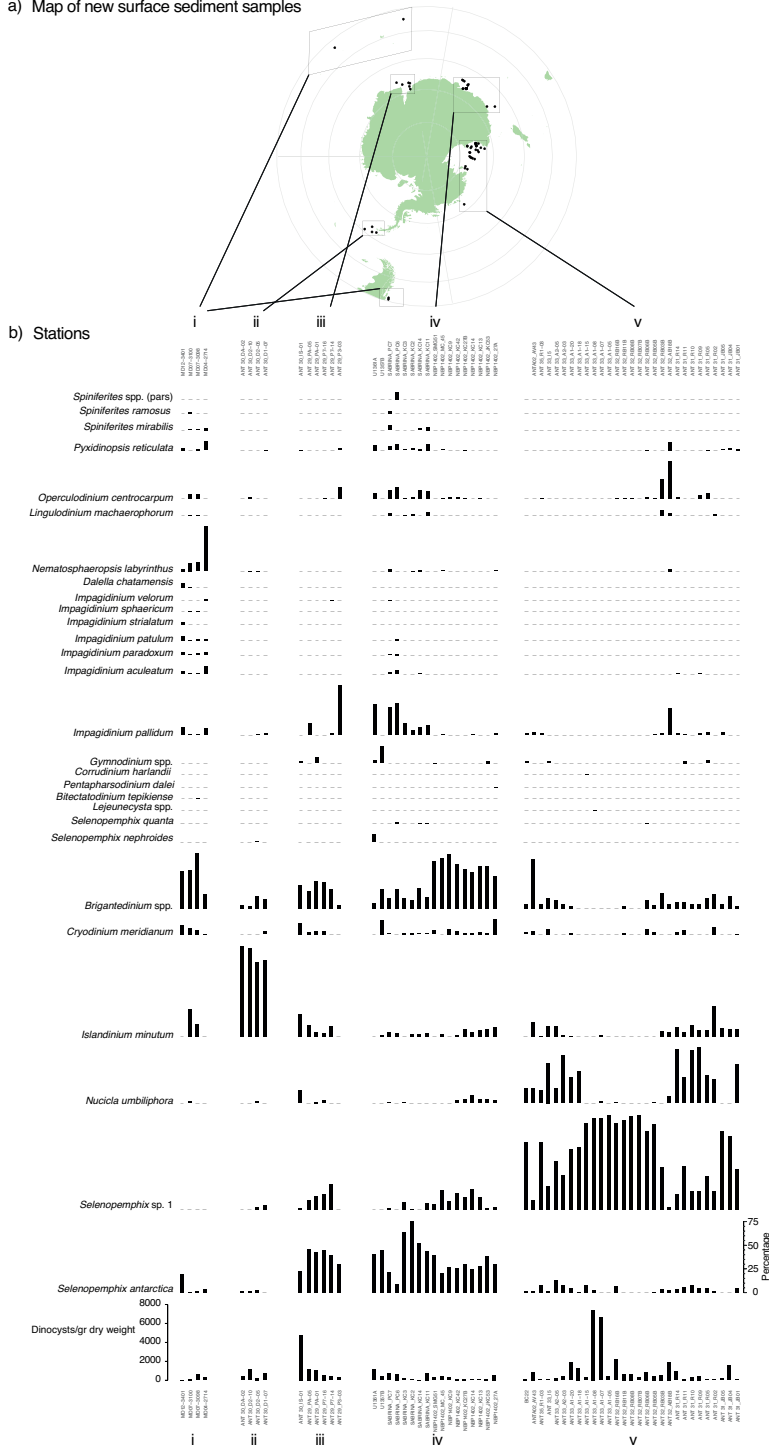
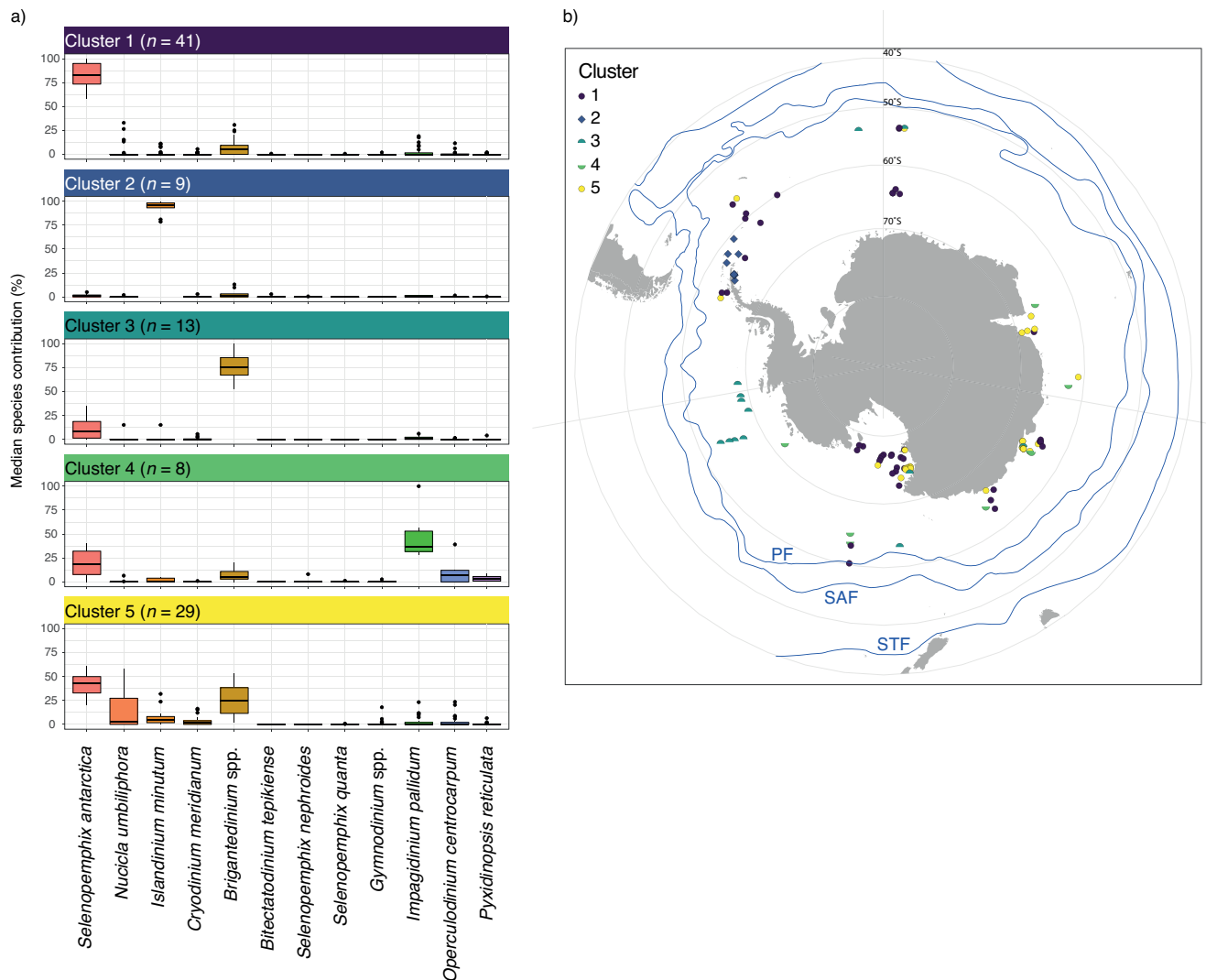


Figure 3: Overview of new counted samples. a) Map of locations of new samples, b) dinocyst assemblages and absolute abundances (in cysts/gram dry weight) for the new samples from the subantarctic/subtropical zone (i), Antarctic Peninsula (ii), Prydz Bay (iii), Sabrina/Wilkes Coast (iv) and Ross Sea (v).

4.3 Clustering of the wsi_100 dataset: the Antarctic proximal sites

K-means clustering of the dinocyst assemblages in the surface sediment samples allow grouping of samples with similar dinocyst assemblages. The most stable solution for the wsi_100 dataset has 5 clusters (Fig. S2; Fig. 4).

- 275 1) **Cluster 1** ($n = 41$) is dominated by *Selenopemphix antarctica*, with few *Brigantedinium* spp., *Operculodinium centrocarpum*, *Nucicla umbiliphora*, *Cryodinium meridianum* and *Islandinium minutum*. Most samples are from the Ross Sea, some along the Sabrina coast or in West Antarctica (Fig. 4b, dark blue).
- 280 2) **Cluster 2** ($n = 9$) consists of nine samples and is strongly dominated by *Islandinium minutum* (Fig. 4a), making up almost 100% of the average assemblage in this cluster. Only very few other species appear in this cluster, most often *Brigantedinium* spp. and *Selenopemphix antarctica*. Samples in this cluster are located in the Weddell Sea (Fig. 4b, blue).
- 285 3) **Cluster 3** ($n = 13$) has samples dominated by *Brigantedinium* spp. Other species, such as *Selenopemphix antarctica*, *Cryodinium meridianum*, *Impagidinium pallidum* and *Islandinium minutum* are rare. Except for one sample in the Ross Sea, Cluster 3 samples are located the furthest away from the Antarctic continent and north of 70°S, mainly appearing in the Pacific Ocean sector (Fig. 4b, green).
- 4) **Cluster 4** ($n = 8$) has abundant *Impagidinium pallidum*. *Selenopemphix antarctica* is common with few *Brigantedinium* spp., *Operculodinium centrocarpum*, and *Pyxidinosia reticulata*. Samples from this cluster appear everywhere around Antarctica with no clear restrictions or affinities (Fig. 4b, bright green). They are located within the Ross Sea, Weddell Sea but also further away from the Antarctic continent.
- 290 5) **Cluster 5** ($n = 29$) has abundant to dominant *Selenopemphix antarctica*. *Brigantedinium* spp. is common, as are *Nucicla umbiliphora*, *Cryodinium meridianum* and *Islandinium minutum*. Samples of this cluster are located in the Ross Sea, Prydz Bay and along Sabrina Coast, mostly close to the coast (Fig. 4b, yellow).



295 **Figure 4: 5-cluster solution for the wsi_100 dataset (considering all sample locations that experience surface winter (JJA) sea ice). A) The dinocyst assemblages for each cluster (showing only the main 12 dinocyst species) and b) locations of samples color-coded by different clusters. Also plotted are frontal systems (blue lines, STF = Subtropical Front, SAF = Subantarctic Front, PF = Polar Front). Black horizontal line depicts the median, the coloured box the 25% and 75% quantile, and the whiskers the 95% confidence interval.**

4.2 Clustering of the sh_655 dataset

300 The 9-cluster result of our *k*-means cluster analyses offers the most stable solution for the sh_655 dataset (Fig. 5; Fig. S3). Below is the median dinocyst assemblage for each cluster.

- 1) **Sant-Cluster** ($n = 64$): *Selenopemphix antarctica* dominates (Fig. 5a). *Nucicla umbiliphora*, *Islandinium minutum*, *Cryodinium meridianum* and *Brigantedinium* spp. are common. *Impagidinium pallidum* and *Operculodinium*

centrocarpum are rare. All 64 samples in this cluster are located near the Antarctic continent, such as in the Ross Sea, offshore the Sabrina Coast and in Prydz Bay (Fig. 5b).

- 2) **Imin-Cluster** ($n = 9$): Dinocyst assemblages in this cluster are strongly dominated by *Islandinium minutum* (Fig. 5a). Other species such as *Brigantedinium* spp. are rare. Although only very few samples (9) belong to this cluster, all located in the Weddell Sea (Fig. 5b), it separates out from the other samples in all cluster solutions (see supplementary figures). This cluster is the same as the first cluster in the wsi_100 dataset (Fig. 4).
- 3) **high-Brig-Cluster** ($n = 86$): This cluster is dominated by *Brigantedinium* spp. Assemblages are quite diverse, with few *Selenopemphix quanta*, various *Impagidinium* species, *Nematosphaeropsis labyrinthus*, *Operculodinium centrocarpum* or *Spiniferites* species.
- 4) **Nlab-Cluster** ($n = 72$): *Nematosphaeropsis labyrinthus* is abundant, with common *Brigantedinium* spp.. Several other species, such as *Impagidinium* species, *Selenopemphix quanta* and *Selenopemphix nephroides*, *Operculodinium centrocarpum*, *Pyxidinosia reticulata*, *Dalella chathamensis* (in highest numbers of all clusters) and *Spiniferites mirabilis* occur in low abundance. Samples are located between 40 and 60°S, most prominently south(-west) of Tasmania and New Zealand, but also in the Indian Ocean and along the South American West coast.
- 5) **low-Brig-Cluster** ($n = 120$): *Brigantedinium* spp. is common in this cluster. Samples also contain few to common *Operculodinium centrocarpum*, *Nematosphaeropsis labyrinthus*, *Impagidinium* and *Spiniferites* species as well as *Selenopemphix quanta* and *Selenopemphix nephroides*. Other P-cysts such as *Selenopemphix antarctica*, *Nucicla umbiliphora*, *Islandinium minutum* and *Cryodinium meridianum* are rare. Samples' locations have a wide geographic spread, but many are located around New Zealand (closer to the coast than samples from other clusters), south of Australia and around Tasmania (but in low numbers), in mid-latitudes along the west coast of Africa, and along the west coast of South America. Also, samples can occasionally be found in the open ocean, for example the Indian Ocean or close to Antarctica.
- 6) **low-Ocen-Cluster** ($n = 115$): no single species clearly dominates the assemblage, yet *O. centrocarpum* is common to abundant. Almost all common 20 species can be present in samples of this cluster. Samples contain few *Brigantedinium* spp., while other species have strongly variable abundance, such as *Impagidinium pallidum*, other *Impagidinium* species, *Nematosphaeropsis labyrinthus* and *Spiniferites* spp. The geographic distribution of samples within this cluster is scattered: samples are in the Ross Sea and all along ice-proximal sites around Antarctica, but also in mid- and low latitudes, in coastal areas as well as in open ocean conditions. No clear geographical distribution is apparent.
- 7) **Iacu-Cluster** ($n = 58$): *Impagidinium aculeatum* is abundant. Samples also contain few other *Impagidinium* species, *Nematosphaeropsis labyrinthus*, *Operculodinium centrocarpum*, and *Brigantedinium* and *Spiniferites* species. The samples of this cluster are mostly found between 40° and 20°S, although some samples are located even closer to the equator (in the Atlantic Ocean).

8) **High-Ocen-Cluster** ($n = 72$): This cluster is dominated by *Operculodinium centrocarpum* with few *Brigantedinium* spp., *Nematosphaeropsis labyrinthus*, *Spiniferites mirabilis* and *Spiniferites* spp. Many other species occur in low abundance. Most samples of this cluster can be found close to the continental coasts of South Africa, Australia, and South America.

340

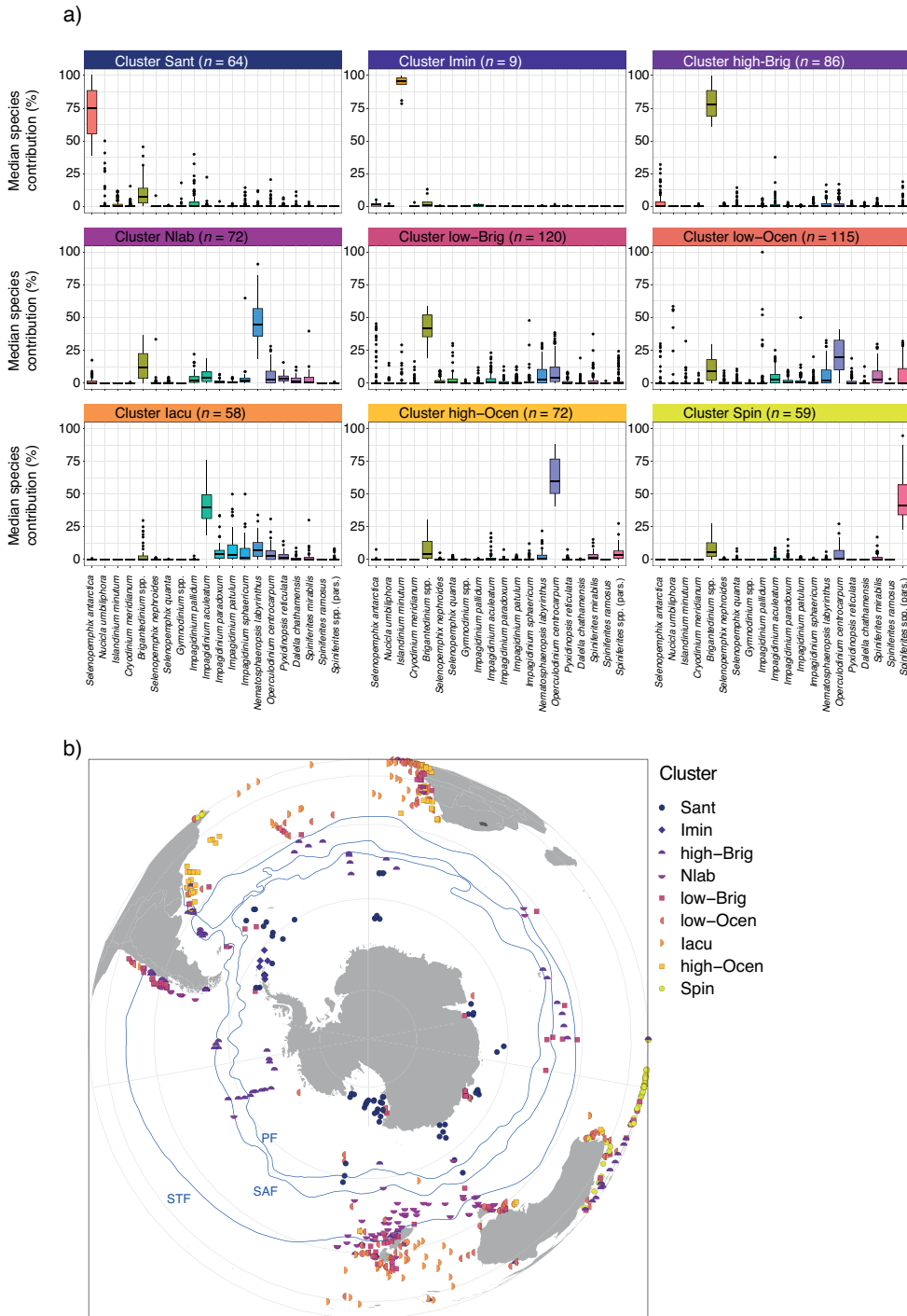
9) **Spin-Cluster** ($n = 59$): *Spiniferites* species are abundant, with few *Brigantedinium* spp. and *Pyxidinopsis reticulata*, as well as *Impagidinium* species (*I. aculeatum*, *I. patulum* and *I. sphaericum*) and *Selenopemphix quanta*. Most samples are located along the north-west coast of Australia and in low latitudes in the eastern Indian Ocean.

345 4.4 Comparison between clusters and environmental parameters

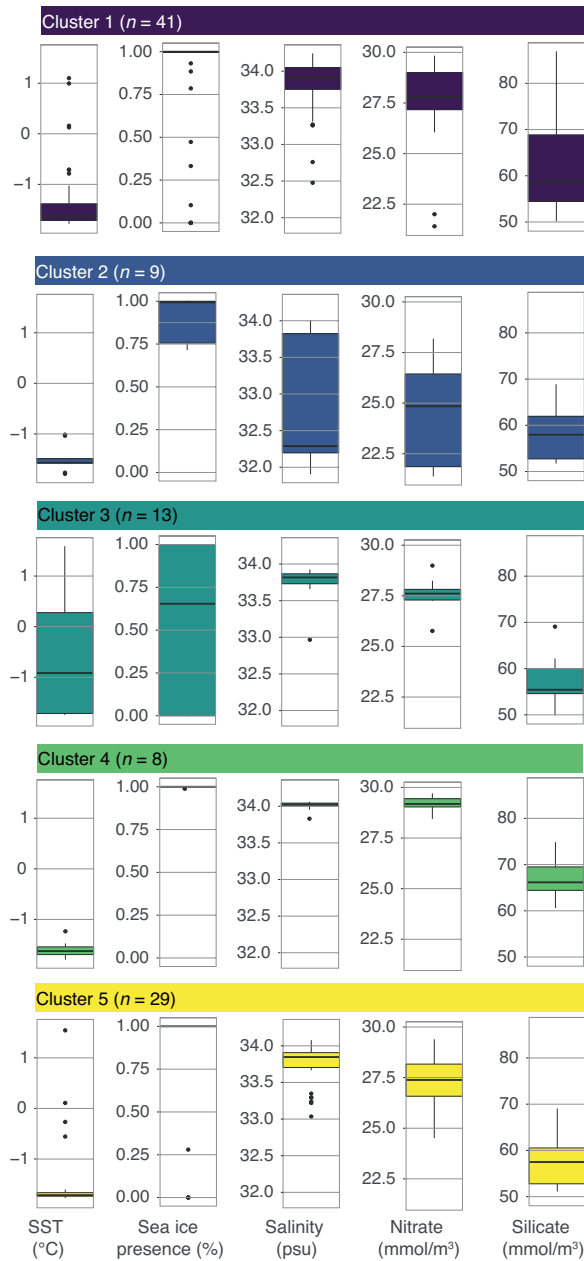
4.4.1 wsi_100: directly overlying water only

Overall, differences in oceanographic conditions are relatively small when considering the samples from the Antarctic proximal sites: nutrients are overall high, sea-ice presence is almost 100% and sea-surface temperature is low (average -1.5°C), but some differences between the clusters can be identified (Fig. 6). Salinity is generally between 33.6 and 34 psu in samples from all clusters, except for Cluster 2 that has a lower median of 32.3 psu. Cluster 3 includes samples within the largest SST range ($-1.4 - 0.2^{\circ}\text{C}$; Fig. 6) and lowest sea-ice presence (median <0.7) compared to the other clusters. Cluster 1, 4, and 5 have overall very similar conditions. This means that the common *Impagidinium pallidum* in samples from Cluster 4 cannot be directly associated to any environmental parameters considered here.

350



355 **Figure 5: 9-cluster solution for the sh_655 data set. A) The dinocyst assemblages for each cluster (showing only the main 20 dinocyst species). Line, box and whiskers as in Fig. 3. b) locations of samples color-coded by different clusters and frontal systems (blue lines, STF = Subtropical Front, SAF = Subantarctic Front, PF = Polar Front).**

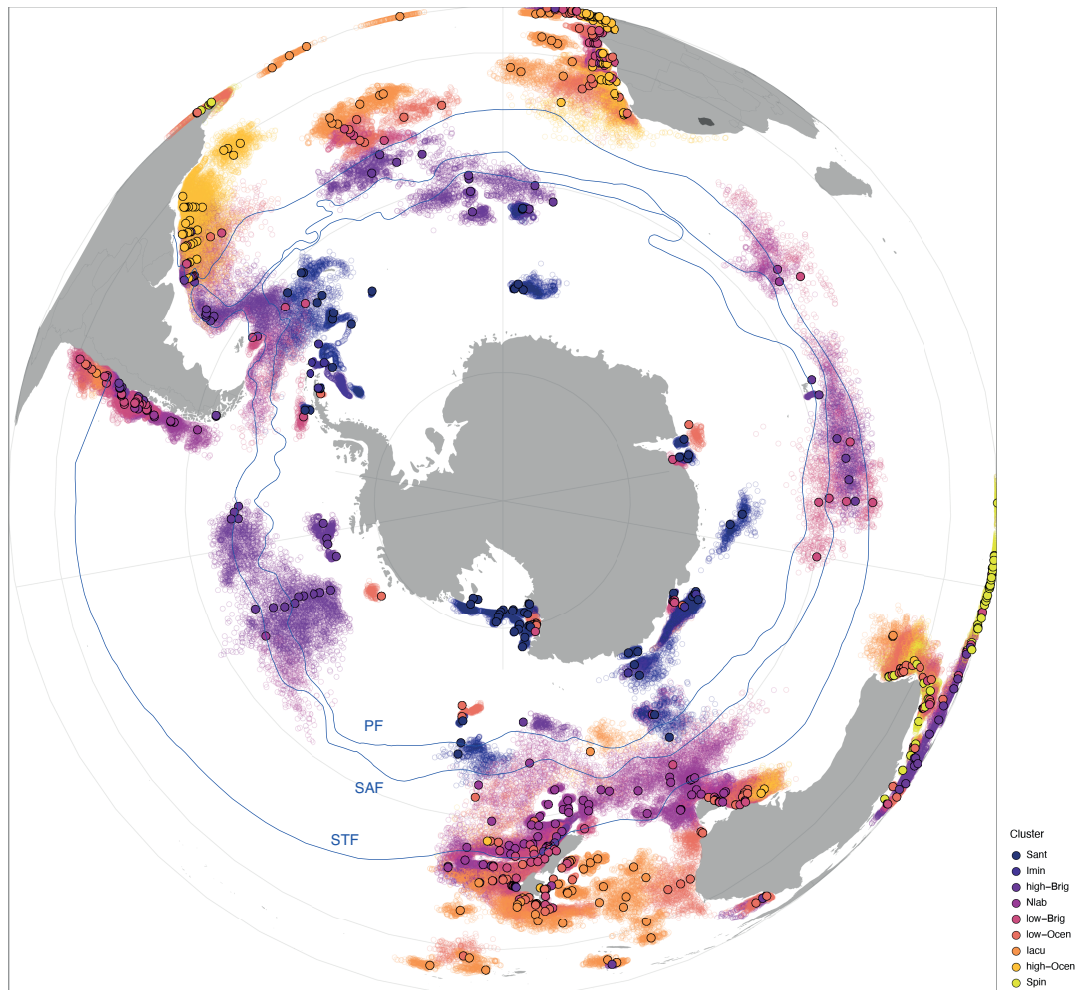


360 **Figure 6: Environmental parameters for the 5-cluster solution for the wsi_100 data set. The median (black line) of all observations per cluster (1–5), with the 25% and 75% quantile as box and whiskers as 95% confidence interval. Single points represent outliers.**

4.4.2 sh_655 – surface versus transport

To better attribute environmental parameters to the clusters in sh_655, we compare the overlying surface water conditions of each location with that of modelled lateral particle (dinocyst) transport area due to ocean currents. Taking lateral transport into

365 account, the source region for particles (dinocysts) is, for some samples, non-randomly offset from the directly overlying
water. In the Southern Ocean south of the Subtropical Front, most transport is zonal and not meridional, because of prevailing
zonal direction of currents. Regardless of their assigned cluster, all samples that are located between 40 and 60°S have a
westward-displaced surface water source region (Fig. 7). For the Imin-cluster, the source regions from the lateral transport are
confined to the Weddell Sea. For the Sant-cluster, the surface areas of samples in the Ross Sea are not displaced much when
370 lateral transport is accounted for. Dinocysts in the samples from Sabrina Coast and Prydz Bay are originated slightly more
eastwards. In general, for the Iacu-cluster, the source regions are large, but do not show a clear bias to latitudinal or longitudinal
transport. These source regions reflect the ocean-current dictated provincialism (Fig. 7) as recently indicated by similar particle
trace experiments (Nooteboom et al., 2022).



375 **Figure 7: Location and source regions of samples. Overview map of sample locations (filled dots) color-coded by cluster with modelled backtracked transport surface-ocean origin (open dots). Also plotted are frontal systems (blue lines, STF = Subtropical Front, SAF = Subantarctic Front, PF = Polar Front)**

We compare the differences in oceanographic conditions in the median overlying surface water for each cluster in the sh_655 dataset. This can be further compared to the median conditions of the wider region after taking lateral transport into account (Fig. 8). Most clusters have distinct differences in oceanographic conditions of the directly overlying water. The differences between the oceanographic conditions in the overlying water and the lateral transport region are overall small for most clusters and parameters, but some peculiarities do appear:

- In the Sant-cluster, there are hardly differences between the directly overlying water and the lateral transport area. The average sea-surface temperature is -1.7°C , and the median sea-ice presence is at 100%. Here, the transport data shows a much larger range (below 50%) than the overlying data (below 75%). Salinity is around 33.8 psu and nitrate and silicate concentrations are quite high (around 27.5 and 56–57 mmol/m^3 , respectively).
- In the Imin-cluster, the average sea-surface temperature for the overlying water is around -1.6°C , and sea-ice presence is almost at 100%. In the transport data, SST is around -1.7°C , and sea ice presence is at 100%. There are more striking differences between overlying and transport data in salinity, nitrate, and silicate concentrations. For salinity, the overlying data shows an average of around 32.3 psu with a quite large range, whereas the transported data shows a much more constrained value around 33.9 psu. Nitrate and silicate concentrations in the overlying data show values around 25 and 58 mmol/m^3 , respectively. The transported data show values around 28 and 63 mmol/m^3 , respectively.
- In the high-Brig-cluster, overlying and transport data depict similar values. Sea-surface temperature for both data is around 10°C , sea ice is not present (only as outliers), and salinity is around 34.1 psu. Nitrate and silicate concentrations are relatively high (around 16 mmol/m^3). Compared to other clusters, the range is relatively large.
- In the Nlab-cluster, the average sea-surface temperature for both overlying and transported datasets is around $11\text{--}12^{\circ}\text{C}$, sea ice is not present, except in two samples. Salinity is around 34.4 psu. Nitrate concentrations are around 15 mmol/m^3 and silicate concentrations are around 12 mmol/m^3 .
- In the low-Brig-cluster, the average sea-surface temperature for both data is around 15°C . Sea ice is not present, and salinity is around 34.5 psu. Nitrate and silicate concentrations are rather low (just above 10 mmol/m^3 and below 5 mmol/m^3 , respectively).
- In the low-Ocen-cluster, overlying and transport data depict similar values. The average sea-surface temperature for both data is around 18°C , sea ice is not present, and salinity is around 35.4 psu. Nitrate and silicate concentrations are very low ($< 5 \text{ mmol}/\text{m}^3$).
- For the Iacu-cluster, overlying and transport data are again almost identical. Sea-surface temperature for both data is around 22.5°C , and sea ice is not present. Salinity is around 35.5 psu and nitrate and silicate concentrations are very low ($< 2 \text{ mmol}/\text{mmol}/\text{m}^3$). The range in this cluster is very small.
- In the high-Ocen-cluster, the average sea-surface temperature for both data is around 22°C . Sea ice is not present, and salinity is around 35.5 psu. Nitrate and silicate concentrations are very low ($< 2 \text{ mmol}/\text{m}^3$). The range in this cluster is relatively narrow for all parameters.

- In the Spin-cluster, the average sea-surface temperature for both data is around 29°C. Sea ice is not present, and salinity is just below 34 psu. Nitrate and silicate concentrations are exceptionally low (below 0.1 and 1 mmol/m³, respectively). The range in this cluster is very narrow for all parameters.

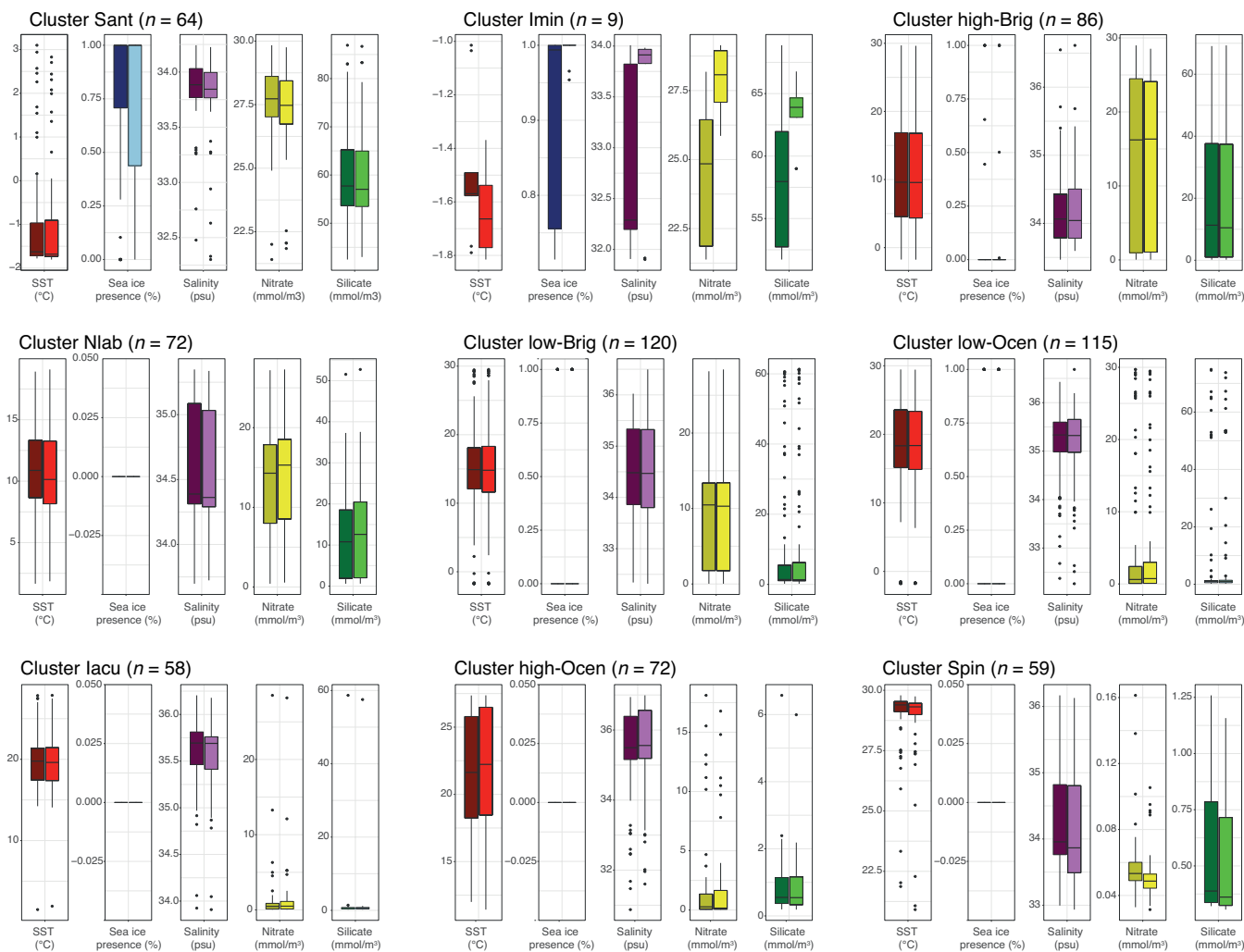


Figure 8: Comparison of environmental parameters for the 9-cluster solution in the SH_655 data set. For each cluster (Fig. 5), we compare the environmental parameters SST (red), sea ice presence (blue), salinity (purple), nitrate (yellow) and silicate (green) of the directly overlying surface waters (left-side bar, darker fill) to those resulting from the particle transport (right-side bar, lighter fill). Black line, box and whiskers as in Fig. 6.

5.1 Dynamics at ice-proximal sites: dinocysts as sea-ice proxy

The better representation of Antarctic ice-proximal sites in our new dataset allows to further examine Antarctic dinocyst assemblages and associated environmental dynamics, which will help constraining paleoreconstructions. The dominance of *Islandinium minutum* in Weddell Sea locations is very striking (Figs. 3, 4). In the wsi_100 dataset, nine samples with high *I. minutum* percentages form their own cluster (Fig. 4). The cluster persists when the entire “sh_655” dataset is considered (Fig. 5). This suggests that regionally unique environmental conditions strongly favor the presence of *I. minutum*. The source region for these samples can be placed in the Weddell Sea, suggesting that *I. minutum* may be transported from the Weddell Sea towards the tip of the Antarctic Peninsula along with the icebergs (“Iceberg Alley”; Fig. 7). The low salinities of the surface waters overlying Imin cluster samples further suggests a major influence of icebergs and associated melting as the values are the lowest of all clusters (Fig. 6; also, in the sh_655 dataset, Figs. 8 & 9). It seems that *I. minutum* dominates the assemblage in low and/or seasonally variable salinity and can thus thrive under these conditions, outcompeting other species. Other conditions such as SST, sea-ice presence, and nutrient concentrations, although slightly lower than in the other clusters, should still be high enough to promote blooms of primary productivity. As icebergs and mixing deliver enough micronutrients, there is no (local) iron-limitation expected. Hence, we suggest that a high abundance/dominance of *I. minutum* represents strongly changing and/or relatively low salinity due to the influence of melt water in conditions otherwise typical for ice-proximal sites. Low salinity signals might also appear very locally restricted/punctuated in regions of high sea-ice presence, thus explaining the sparse occurrences of *I. minutum* in other clusters (Fig. 4).

Apart from this, there are no clear regional differences in the dinocyst abundance (Fig. 4) or clustering of the wsi_100 dataset (Fig. 6). The merging of both *Selenopemphix antarctica* varieties in the wsi_100 dataset limits a better distinction of the clusters (Fig. 4). Two clusters are dominated by (varying contributions of) *S. antarctica* (Clusters 1 & 5). Taking our newly counted samples into account in which we separate *S. antarctica* into two varieties (Fig. 3), Cluster 5 mostly consists of *Selenopemphix* sp. 1. Also, *S. antarctica* dominates an assemblage alone, whereas *Selenopemphix* sp. 1 occurs with *Nucicla umbiliphora* (Figs. 3 & 4). Yet, no clear geographic nor environmental component can explain this difference (Figs. 3, 4 & 6). If at all, one could argue that *Selenopemphix* sp. 1 – *N. umbiliphora* occur closer to the coast in the Ross Sea (Fig. 4). This might indicate that *S. antarctica* is constrained tighter to polynya conditions. Yet, there is no polynya vs. closer-to-coast gradient visible in the environmental parameters (Fig. 6). Hence, it remains difficult to attribute environmental conditions to the separate clustering. A better distinction of *S. antarctica* varieties might help to further constrain the differences, although the distinction of *S. antarctica* into subspecies itself remains uncertain.

Despite this, a continuous sea-ice presence in these two clusters argues for a high sea-ice affinity of *S. antarctica* as well as *N. umbiliphora*. This suggests that the species live either directly at the sea-ice edge or in polynya dependent on sea ice-driven conditions. Here, a short growth season in which micro- and macronutrients become available in an essentially unlimited amount (Swailethorp et al., 2019) fuels phytoplankton growth allowing these heterotrophic dinoflagellate species to thrive.

Clusters 3 & 4 include locations furthest away from the Antarctic continent and display a dominance of *Brigantedinium* spp. and *Impagidinium pallidum*, but with lower numbers of *S. antarctica* (and *N. umbiliphora*) (Fig. 4). For Cluster 3, larger ranges
455 for SST and sea-ice presence (Fig. 6) can be translated to seasonal (winter) sea-ice presence and (relatively longer) ice-free summers. We interpret this as a region where the sea-ice season is no longer the sole oceanographic factor influencing productivity. The geographic range and high nutrient concentrations (nitrate and by inference silicate) indicate that these locations are influenced by strong vertical mixing delivering (micro- and) macro-nutrients to the surface ocean.

This opens the question as to when low numbers of *S. antarctica* (or *N. umbiliphora*) should be considered as a signal of low
460 sea-ice presence or as a transport signal (Nooteboom et al., 2019) in paleo-reconstructions. Again, we argue to consider the entire dinocyst assemblage. If the assemblage is dominated by species such as *Brigantedinium* spp., *Impagidinium pallidum*, or *Operculodinium centrocarpum*, with broad environmental niches and occurrences, we suggest considering *S. antarctica* and *N. umbiliphora* as indicator of low (seasonal) sea-ice presence. In contrast, if *S. antarctica* and *N. umbiliphora* exist in assemblages dominated by *N. labyrinthus*, *I. aculeatum* or *Spiniferites* spp., we argue for a transport signal, since in our
465 clusters, *S. antarctica* and *N. umbiliphora* are completely absent when sea-ice is absent (Figs. 5, 9 and 10). Note that this transport includes that of deep-ocean and bottom currents which are strong in the Southern Ocean subsurface (see Nooteboom et al., 2019). Consequently, the (low) occurrences of *Brigantedinium* spp. in *S. antarctica*-dominated clusters may indicate the high tolerance of that species to sea ice and/or quick growth during (short) ice-free conditions.

5.2 SH_655 dataset: representation of Southern Hemisphere frontal zones

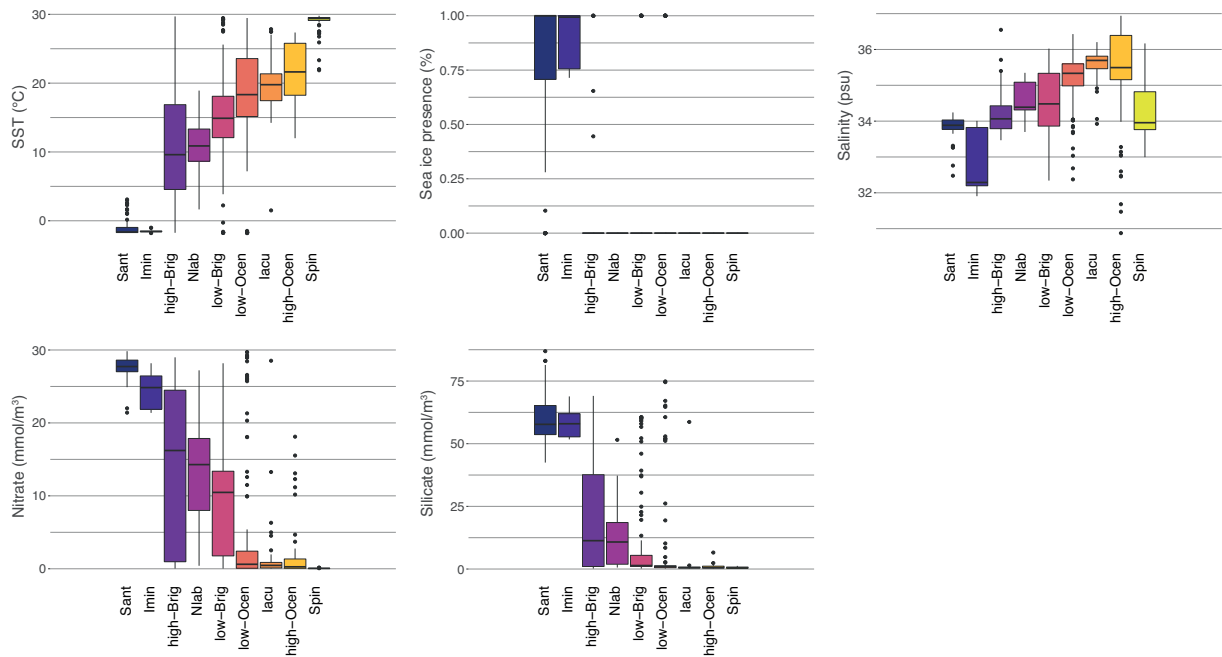
470 Compared to previous studies (e.g., Prebble et al., 2013), our study has additional surface sediment samples on both extreme ends: the warm low-latitude end as well as the cold, sea ice-influenced, polar end. As a result, the current sediment sample set better represents the full suite of Southern Hemisphere surface oceanographic conditions. From the pole towards the equator, the clusters depict a gradual warming, and decrease in nitrate and silicate concentrations (Fig. 9), as seen in the modern oceanographic conditions (Fig. 1). The sea ice-influenced zone is represented by samples from the summer and winter sea-ice
475 edge, from regions affected by polynya (e.g., Ross Sea and Weddell Sea) and icebergs (Antarctic Peninsula). On the warm end, the Spin-cluster is a representation of warm, low-salinity but also surprisingly low-nutrient surface waters, possibly impacted by high precipitation rates (Fig. 9).

The depicted gradients in the Southern Hemisphere oceanographic conditions can be assigned to key zones in the Southern Hemisphere surface ocean, with specific oceanographic parameters (Figs. 1, 9), clearly represented by the dinocyst assemblage
480 clusters (Fig. 5). It must be noted here that, although these clusters are characterized by one or two dominant taxa, assigning ecological affinity from assemblages should consider the full context of the dinocyst assemblage(s).

- Antarctic Zone: Sant- and Imin clusters. The Antarctic Zone is clearly characterized by an abundance of P-cysts, with dominance of *Selenopemphix antarctica* and/or *Islandinium minutum*. These are the only two clusters with significant sea-ice presence and SST below 0°C. Together with high nutrient conditions, these two clusters clearly depict the AZ
485 conditions of upwelling, vertical mixing, and sea-ice influence. Potentially, the high nutrient concentrations can fuel

phytoplankton growth that the dominant dinocyst species can feed on then. However, we cannot confirm if *S. antarctica* and/or *I. minutum* thrive under/at the edge of sea-ice conditions and could thus be used as a sea-ice proxy. The cluster also includes samples further away from the Antarctic continent (Fig. 5b), where the influence of sea ice might be limited, but cold SST and high nutrient conditions prevail. Thus, a quantitative estimate for past sea ice seems difficult. On the other hand, sea-ice dominated regions like the Ross Sea, Prydz Bay, and the Sabrina Coast contain samples with high abundances of *S. antarctica* and argue that this species might be at least best adapted to sea-ice conditions. The largest difference between these two clusters can be found in their salinity range (Fig. 9). Regions within the sea-ice zone dominated by *I. minutum* have substantially lower salinity than those dominated by *S. antarctica* and as such, dominance of *I. minutum* might be taken as a low-salinity indicator in cold, sea ice-prone environments (see section 5.1).

- Subantarctic zone: Nlab-cluster. The Subantarctic Zone is very well depicted by the Nlab-cluster, dominated by *N. labyrinthus*. Besides that, *Brigantedinium* spp., but also other P- or G-cysts (*Impagidinium* species) might show up in small numbers. The environmental parameters of this cluster are characteristic of the SAZ (Fig. 9). Although the environmental parameter profile and occurrence of many dinocyst species might indicate a transitional character of this zone, the SST range compared to other distinctly zonal cluster is quite narrow. Similarly, the STF can be very clearly made out as the northern boundary for this cluster and high numbers of *N. labyrinthus* occurrences (Fig. 5b), best seen around Australia/Tasmania and New Zealand.
- North of the Subtropical Front: Iacu- and Ocen-cluster. The clusters that describe best the conditions just north of the STF are the Iacu-cluster with *I. aculeatum* and the Ocen-clusters with *O. centrocarpum* being the dominant species. The trends of increased SST and salinity due to higher evaporation continue, and nutrient availability drops to almost zero, characteristic for sub-tropical conditions that are less influenced by Southern Ocean/ACC-conditions. The environmental difference between these two clusters is difficult to discern. It seems that samples of the Ocen-cluster have slightly higher nitrate (and silicate) concentrations and lower salinity (Fig. 9). For the high-Ocen-cluster, this might be caused by samples of the cluster being located closer to land (Fig. 5b). This might argue for *I. aculeatum* needing slightly more open-ocean conditions. Besides, considering the much narrower environmental parameter ranges in the Iacu-cluster, this might indicate that *I. aculeatum* can dominate the assemblage in a quite specific range and is outcompeted by the generalist *O. centrocarpum* if conditions are not optimal. Nevertheless, the drastic assemblage changes from the *N. labyrinthus*-dominance south of the STF to the *I. aculeatum*- or *O. centrocarpum* dominance north of the STF might be used to track STF positional shifts in the past. While many clusters (due to the doubled sample size, see Table 1) differ a lot from clusters found by (Prebble et al., 2013), this Nlab-vs-Iacu-distinction at the STF was also observed there.
- Warm low latitudes: Spin-cluster. The cluster dominated by *Spiniferites* spp. appears in very low latitudes and/or locally very warm areas, such as the Australian west coast (Fig. 5), confirmed by almost 30°C SST. Striking is also the lower salinity, which breaks the increasing trend for the clusters before.



520

Figure 9: Comparison of environmental surface conditions in different clusters for the 9-cluster solution of the sh_655 data set. The median, 25% – 75% quantiles and 95% confidence interval is indicated by the black line, boxes and whiskers, respectively, for environmental parameters SST (°C), sea ice presence (%), salinity (psu), nitrate and silicate (mmol/m³) for each cluster color-coded as in Fig. 5. The environmental conditions of the directly overlying water are used here, as particle transport does not cause large differences in the environmental ranges of the clusters (see Fig. 8).

525

The 9 clusters are mostly well defined to different zones and regions in the Southern Hemisphere. However, there seems to be a gap remaining in the 0–8°C SST range, that is partly covered by either the polar clusters and/or the high-Brig-cluster. This SST range also includes the transitional zone between 0 and 100% sea ice presence. Better geographical representation of this transitional zone in surface sediment sample sets might improve constraining this transitional zone.

On the other hand, it might be that the nature of this part of the Southern Ocean, with large scale turbulent mixing will keep causing a mixed dinocyst assemblage. The large ranges of the high-Brig-cluster in SST, but also in nutrient concentration (Fig. 9) might best represent this dynamic environment, with *Brigantedinium* spp. as more generalist species dominating the dinocyst assemblage (Fig. 5). This is also the case for the low-Brig-cluster, that does not show any clear oceanographic boundaries. Potentially, conditions that (temporarily) disadvantage the dominance of the expected dinocyst might allow for *Brigantedinium* spp. to take over and thrive. Yet, the difference between the low- and high-Brig-cluster in terms of SST, but also nutrient conditions, might argue for a high *Brigantedinium*-tolerance to cold and very dynamic Polar Frontal Zone conditions (Figs. 4, 9).

530

535

5.3 The impact of lateral transport

540 The size of the surface areas represented in the sample stations, as visualized in Fig. 7, suggests that many areas in the Southern Ocean are impacted by transport (see also Nooteboom et al., 2019). This is especially true for samples located within the ACC. For these locations, their source regions are consistently placed to the west, implying that the strong ACC current transports particles clockwise, eastward around Antarctica. South of the direct influence of the ACC, the source region is displaced farther towards the east due to the counter-clockwise Antarctic Coastal Current. Other features that are recognizable are the Agulhas

545 Leakage, transporting particles along the east coast of South Africa into the Atlantic Ocean, and the so-called ‘Iceberg Alley’. This area is known for a high number of icebergs drifting along the west coast and eventually out of the Weddell Sea due to the Weddell Gyre. Locations that are not directly influenced by the ACC and these smaller features do not experience such a large transport. Thus, ice-proximal and low-latitude (north of ~40°S) sites experience relatively little transport. This can mostly be attributed to the absence of strong currents and coastal proximity.

550 Overall, zonal transport is much stronger than meridional. This does not exclude latitudinal transport (Nooteboom et al., 2019), but does limit its influence. Environmental conditions are not hugely different on a zonal scale as they are meridional, which suggests that cysts preserved in sediments can be generally linked to overlaying surface water conditions. The comparison of environmental parameters between particle transport and overlying surface for the different clusters confirms this assumption (Fig. 8). Transport does not affect the environmental affinities of the clusters significantly. The only exception is the Imin-

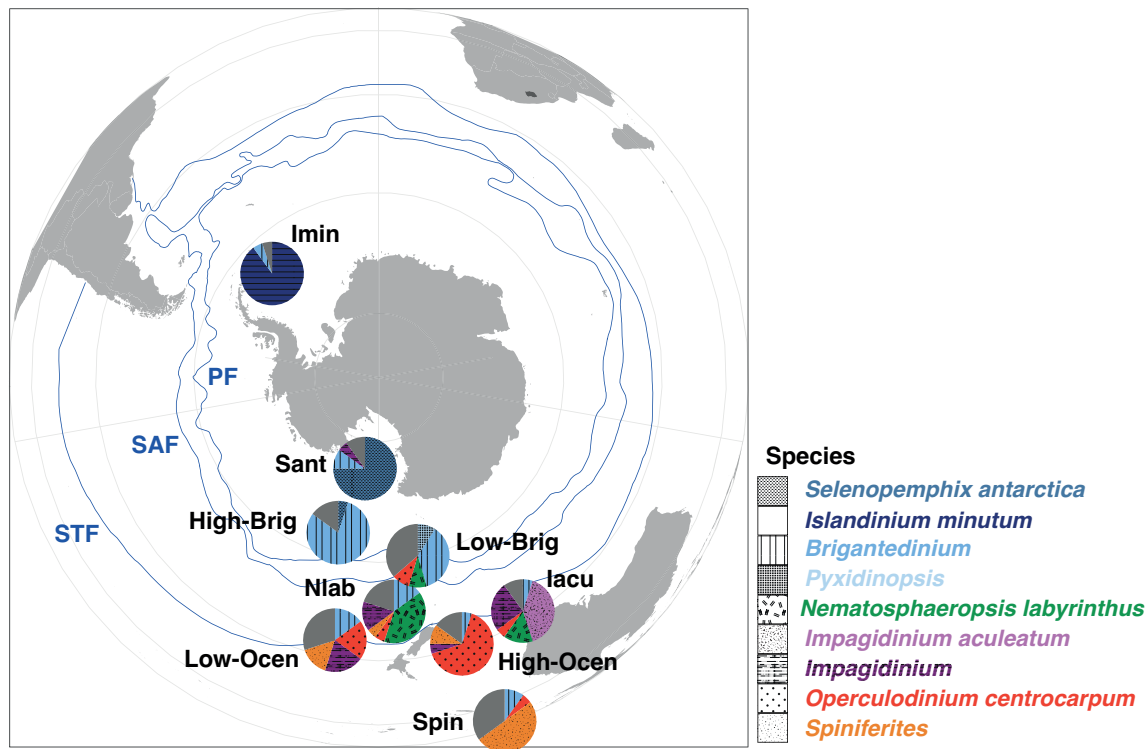
555 cluster, that clearly shows the influence of transport along the “Iceberg Alley”. The source region of the particles is predominantly the Weddell Sea, hence the cluster represents narrower environmental conditions (Fig. 8).

5.4 Dinocyst assemblages as proxy for Southern Ocean frontal systems

For the regions in the Southern Ocean that were already well-represented in previous surface sediment compilations (e.g., Prebble et al., 2013), our additional samples do not require changing earlier interpretations. Distinct dinocyst assemblages

560 exist on either side of the front systems in the Southern Ocean (Fig. 10). For the Subtropical Front, the difference is mostly observed between the Nlab-cluster in the SAZ and Ocen-or Iacu-cluster north of the STF. These clusters are promising as proxies for depicting the paleolocation of the STF relative to the position of sediment records: high abundance of *Nematosphaeropsis labyrinthus* means the STF was north of the study area, whereas high abundance of *Operculodinium centrocarpum* or *Impagidinium aculeatum* indicates that the STF was south of the study area. The few samples available

565 between the SAZ and the PF generates an unclear signal, although it seems like the assemblages transition from abundant Nlab to high-Brig. The latter is associated to the high-nutrient conditions in the Antarctic Divergence.



570 **Figure 10: Schematic representation of the generalized biogeographic distribution of dinocysts in Southern Ocean surface sediments. Pies represent average assemblage composition of the nine clusters described in this paper. Position of these pies represent their typical latitudinal band of occurrence. Also plotted are the frontal systems (blue lines, STF = Subtropical Front, SAF = Subantarctic Front, PF = Polar Front). The Subantarctic Zone (SAZ) is the water mass between the STF and PF.**

6. Conclusion

This study fills a gap in the knowledge of dinocyst assemblage environmental preferences, specifically from the Antarctic ice-proximal locations. With a more solid framework to qualitatively interpret past oceanographic conditions (sea ice, nutrients, sea-surface temperature, salinity) from Southern Ocean dinocyst assemblages (paleo)reconstructions can now be tightly constrained. The 5 clusters in the ice-proximal assemblages demonstrate regional heterogeneity in sea-ice ecosystems. However, *Selenopemphix antarctica* can be used as sea-ice indicator and assemblages dominated by a combination of *Selenopemphix* sp.1 and *N. umbiliphora* may also be prone to provide information on the length of sea-ice season. *Selenopemphix antarctica* and *Selenopemphix* sp.1 need to be counted separately before further environmental interpretations and conclusions can be made.

580

We interpreted nine clusters on the entire Southern Hemisphere dinocyst database (n=665), which can be broadly related to various oceanographic zones in the Southern Ocean and have clear differences in their oceanographic affinities. Despite strong currents and deep basins, lateral transport of sinking particles has little effect on the relationship between surface oceanographic conditions and sedimentary assemblages. This means that for the clusters, oceanographic conditions of the directly overlying

585 water are a good approximation of what sedimentary plankton assemblages relate to, while lateral transport can influence
sedimentary plankton assemblages at individual sites or when the results of this study are used in paleoreconstructions. From
the results of the entire Southern Ocean dataset and our identified 9 clusters, we identify frontal-zone-specific dinocyst
assemblages, separated by Southern Ocean fronts PF, SAF, STF. Our results provide a solid basis for further use of dinocyst
assemblages as indicator for past oceanographic conditions in the Southern Ocean, including frontal system locations through
590 time.

7. Data availability

Microscope slides are stored in the collection of the Marine Palynology and Paleooceanography group under storage code
000.000.017.533. Dinocyst data (this includes the counts of *Polarella glacialis*, sample weights and *Lycopodium* counts to
calculate absolute concentrations), particle trace model output and various cluster analyses, as well as an R markdown
595 providing the coding for the plots in this paper, are available at Github (Bijl, 2022; <https://github.com/bijlpeter83/SH655/>)
and deposited at Zenodo (DOI:10.5281/zenodo.6786422).

8. Author contributions

PKB designed the research with FS. SH, RW, SN and EM provided new sediment samples. LT and SH analysed the samples.
PN contributed Lagrangian particle trace simulations and interpretation of the model data with IS. All authors collaborated in
600 analysing the results and provided input for the writing of the paper.

9. Acknowledgements

This research was financially supported by the seventh framework programme of the European Research Council (ERC
Starting grant number 802835, OceaNice to PKB). We thank Mariska Hoorweg for analytical support in the GeoLab of the
faculty of GeoSciences. We thank CNR_ISMAR, Bologna and INGV, Pisa, Italia, and predecessors of the International Ocean
605 Discovery Program for providing surface sediment samples for this project. This work was jointly supported by the National
Natural Science Foundation of China (Grants No. 42030401 and 41776191). We thank the 29th and 33rd Chinese Antarctic
Expedition cruise members for retrieving the sediments. The authors wish to thank the CSIRO Marine National Facility (MNF)
for its support in the form of sea time on RV Investigator, support personnel, scientific equipment, and data management. All
data and samples acquired on the voyage are made publicly available in accordance with MNF Policy. The constructive and
610 detailed reviews by Joe Prebble and one anonymous reviewer significantly improved this manuscript.

Supplement 1 contains three Supplementary figures.

References

- Adkins, J. F.: The role of deep ocean circulation in setting glacial climates, *Paleoceanography*, 28, 539–561, <https://doi.org/10.1002/palo.20046>, 2013.
- Armand, L.K., O'Brien, P.E. and On-board Scientific Party. Interactions of the Totten Glacier with the Southern Ocean through multiple glacial cycles (IN2017-V01): Post-survey report, Research School of Earth Sciences, Australian National University: Canberra, 2018 <http://dx.doi.org/10.4225/13/5acea64c48693>
- Behrens, B., Miyairi, Y., Sproson, A. D., Yamane, M., and Yokoyama, Y.: Meltwater discharge during the Holocene from the Wilkes subglacial basin revealed by beryllium isotope analysis of marine sediments, *Journal of Quaternary Science*, 34, 603–608, <https://doi.org/10.1002/jqs.3148>, 2019.
- Bijl, P.K.: SH655 dinocyst surface sediment database, <https://github.com/bijlpeter83/SH655>; last access 01-07-2022; DOI:10.5281/zenodo.6786422.
- Bijl, P. K., Houben, A. J., Hartman, J. D., Pross, J., Salabarnada, A., Escutia, C., & Sangiorgi, F. (2018a). Paleoceanography and ice sheet variability offshore Wilkes Land, Antarctica-Part 2: Insights from Oligocene-Miocene dinoflagellate cyst assemblages. *Climate of the Past*, 14(7), 1015–1033.
- Bijl, P. K., Houben, A. J. P., Bruls, A., Pross, J., and Sangiorgi, F.: Stratigraphic calibration of Oligocene–Miocene organic-walled dinoflagellate cysts from offshore Wilkes Land, East Antarctica, and a zonation proposal, *J Micropalaeontol*, 37, 105–138, <https://doi.org/10.5194/jm-37-105-2018>, 2018b.
- Bromwich, D. H., Carrasco, J. F., and Stearns, C. R.: Satellite Observations of Katabatic-Wind Propagation for Great Distances across the Ross Ice Shelf, *Mon Weather Rev*, 120, 1940–1949, [https://doi.org/10.1175/1520-0493\(1992\)120<1940:sookwp>2.0.co;2](https://doi.org/10.1175/1520-0493(1992)120<1940:sookwp>2.0.co;2), 1992.
- Crosta, X., Etourneau, J., Orme, L. C., Dalaiden, Q., Campagne, P., Swingedouw, D., Goosse, H., Massé, G., Miettinen, A., McKay, R. M., Dunbar, R. B., Escutia, C., and Ikehara, M.: Multi-decadal trends in Antarctic sea-ice extent driven by ENSO–SAM over the last 2,000 years, *Nat Geosci*, 14, 156–160, <https://doi.org/10.1038/s41561-021-00697-1>, 2021.
- Delandmeter, P and E van Sebille (2019), The Parcels v2.0 Lagrangian framework: new field interpolation schemes, *Geoscientific Model Development*, 12, 3571–3584
- De Schepper, S., Fischer, E.I., Groeneveld, J., Head, M.J., Matthiessen, J.: Deciphering the palaeoecology of Late Pliocene and Early Pleistocene dinoflagellate cysts, *Palaeogeography, Palaeoclimatology, Palaeoecology*, 309 (1–2), pp. 17–32, DOI: 10.1016/j.palaeo.2011.04.020, 2011.
- de Vernal A., Henry M., Matthiessen J., Mudie P.J., Rochon A., Boessenkool K.P., Eynaud F., Grøsfjeld K., Guiot J., Hamel D., Harland R., Head M.J., Kunz-Pirrung M., Levac E., Loucheur V., Peyron O., Pospelova V., Radi T., Turon J.-L., Voronina E.: Dinoflagellate cyst assemblages as tracers of sea-surface conditions in the Northern North Atlantic, Arctic and sub-Arctic seas: The new “n = 67” data base and its application for quantitative palaeoceanographic reconstruction, *Journal of Quaternary Science*, 16 (7), pp. 681 – 698, 2001.

- de Vernal, A. de, Eynaud, F., Henry, M., Hillaire-Marcel, C., Londeix, L., Mangin, S., Matthiessen, J., Marret, F., Radi, T., Rochon, A., Solignac, S., and Turon, J.-L.: Reconstruction of sea-surface conditions at middle to high latitudes of the Northern Hemisphere during the Last Glacial Maximum (LGM) based on dinoflagellate cyst assemblages, *Quaternary Sci Rev*, 24, 897–924, <https://doi.org/10.1016/j.quascirev.2004.06.014>, 2005.
- 650 de Vernal, A., de, Radi, T., Zaragosi, S., Van Nieuwenhove, N., Rochon, A., Allan, E., De Schepper, S., Eynaud, F., Head, M.J., Limoges, A., Londeix, L., Marret, F., Matthiessen, J., Penaud, A., Pospelova, V., Price, A., Richerol, T.: Distribution of common modern dinoflagellate cyst taxa in surface sediments of the Northern Hemisphere in relation to environmental parameters: The new n=1968 database, *Marine Micropaleontology*, 159, art. no. 101796. DOI: 10.1016/j.marmicro.2019.101796, 2020.
- 655 Esper, O. and Zonneveld, K. A. F.: The potential of organic-walled dinoflagellate cysts for the reconstruction of past sea-surface conditions in the Southern Ocean, *Mar Micropaleontol*, 65, 185–212, <https://doi.org/10.1016/j.marmicro.2007.07.002>, 2007.
- Evangelinos, D., Escutia, C., van de Flierdt, T., Valero, L., Flores, J. A., Harwood, D. M., Hoem, F. S., Bijl, P., Etourneau, J., Kreissig, K., Nilsson-Kerr, K., Holder, L., López-Quirós, A., and Salabarnada, A.: Absence of a strong, deep-reaching
660 Antarctic Circumpolar Current zonal flow across the Tasmanian gateway during the Oligocene to early Miocene, *Global and Planetary Change*, 208, 10.1016/j.gloplacha.2021.103718, 2022.
- Hahsler, M., Piekenbrock, M., and Doran, D.: dbscan: Fast Density-Based Clustering with R., *J Stat Softw*, 1, 1–30, <https://doi.org/10.18637/jss.v091.i01>, 2019.
- Harland, R. and Pudsey, C. J.: Dinoflagellate cysts from sediment traps deployed in the Bellingshausen, Weddell and Scotia
665 seas, Antarctica, *Mar Micropaleontol*, 37, 77–99, [https://doi.org/10.1016/s0377-8398\(99\)00016-x](https://doi.org/10.1016/s0377-8398(99)00016-x), 1999.
- Hartman, J. D., Bijl, P. K., and Sangiorgi, F.: A review of the ecological affinities of marine organic microfossils from a Holocene record offshore of Adélie Land (East Antarctica), *J Micropalaeontol*, 37, 445–497, <https://doi.org/10.5194/jm-37-445-2018>, 2018.
- Hoem, F.S., Valero, L., Evangelinos, D., Escutia, C., Duncan, B., McKay, R.M., Brinkhuis, H., Sangiorgi, F., Bijl, P.K.:
670 Temperate Oligocene surface ocean conditions offshore of Cape Adare, Ross Sea, Antarctica, *Climate of the Past*, 17 (4), pp. 1423–1442, DOI: 10.5194/cp-17-1423-2021, 2021a.
- Hoem, F.S., Sauermilch, I., Hou, S., Brinkhuis, H., Sangiorgi, F., Bijl, P.K.: Late Eocene-early Miocene evolution of the southern Australian subtropical front: a marine palynological approach, *Journal of Micropalaeontology*, 40 (2), pp. 175–193, DOI: 10.5194/jm-40-175-2021, 2021b.
- 675 Houben, A. J. P., Bijl, P. K., Pross, J., Bohaty, S. M., Passchier, S., Stickley, C. E., Röhl, U., Sugisaki, S., Tauxe, L., Flierdt, T. van de, Olney, M., Sangiorgi, F., Sluijs, A., Escutia, C., Brinkhuis, H., Scientists, E. 318, Dotti, C. E., Klaus, A., Fehr, A., Williams, T., Bendle, J. A. P., Carr, S. A., Dunbar, R. B., Flores, J.-A., González, J. J., Hayden, T. G., Iwai, M., Jimenez-Espejo, F. J., Katsuki, K., Kong, G. S., McKay, R. M., Nakai, M., Pekar, S. F., Riesselman, C., Sakai, T., Salzmann, U.,

- Shrivastava, P. K., Tuo, S., Welsh, K., and Yamane, M.: Reorganization of Southern Ocean Plankton Ecosystem at the Onset of Antarctic Glaciation, *Science*, 340, 341–344, <https://doi.org/10.1126/science.1223646>, 2013.
- Lange, M and E van Sebille (2017), *Parcels v0.9: prototyping a Lagrangian Ocean Analysis framework for the petascale age*, *Geoscientific Model Development*, 10, 4175–4186
- Locarnini, A., R., Mishonov, A. V., Baranova, O. K., Boyer, T. P., Zweng, M. M., Garcia, H. E., Reagan, J. R., Seidov, D., Weathers, K., Paver, C. R., and Smolyar, I.: *WORLD OCEAN ATLAS 2018 Volume 1: Temperature*, 2018.
- Madec, G.: *NEMO ocean engine*, 2016.
- Marret, F., Vernal, A. de, Benderra, F., and Harland, R.: Late Quaternary sea-surface conditions at DSDP Hole 594 in the southwest Pacific Ocean based on dinoflagellate cyst assemblages, *J Quaternary Sci*, 16, 739–751, <https://doi.org/10.1002/jqs.648>, 2001.
- Marret, F., Zonneveld, K.A.F.: Atlas of modern organic-walled dinoflagellate cyst distribution. Review of Palaeobotany and Palynology 125(1–2), 1–200, DOI: 10.1016/S0034-6667(02)00229-4, 2003.
- Marret, F., Bradley, L., Vernal, A. de, Hardy, W., Kim, S.-Y., Mudie, P., Penaud, A., Pospelova, V., Price, A. M., Radi, T., and Rochon, A.: From bi-polar to regional distribution of modern dinoflagellate cysts, an overview of their biogeography, *Mar Micropaleontol*, 101753, <https://doi.org/10.1016/j.marmicro.2019.101753>, 2020.
- Marschalek J.W., Zurli L., Talarico F., van de Flierdt T., Vermeesch P., Carter A., Beny F., Bout-Roumazeilles V., Sangiorgi F., Hemming S.R., Pérez L.F., Colleoni F., Prebble J.G., van Peer T.E., Perotti M., Shevenell A.E., Browne I., Kulhanek D.K., Levy R., Harwood D., Sullivan N.B., Meyers S.R., Griffith E.M., Hillenbrand C.-D., Gasson E., Siegert M.J., Keisling B., Licht K.J., Kuhn G., Dodd J.P., Boshuis C., De Santis L., McKay R.M., Ash J., Browne I.M., Cortese G., Dodd J.P., Esper O.M., Gales J.A., Harwood D.M., Ishino S., Kim S., Kim S., Laberg J.S., Leckie R.M., Müller J., Patterson M.O., Romans B.W., Romero O.E., Seki O., Singh S.M., Cordeiro de Sousa I.M., Sugisaki S.T., Xiao W., Xiong Z.: A large West Antarctic Ice Sheet explains early Neogene sea-level amplitude, *Nature* 600, 7889, pp 450–455, 2021.
- Marshall, J. and Speer, K.: Closure of the meridional overturning circulation through Southern Ocean upwelling, *Nat Geosci*, 5, 171, <https://doi.org/10.1038/ngeo1391>, 2012.
- Mitchell, B. G., Brody, E. A., Holm-Hansen, O., McClain, C., and Bishop, J.: Light limitation of phytoplankton biomass and macronutrient utilization in the Southern Ocean, *Limnol Oceanogr*, 36, 1662–1677, <https://doi.org/10.4319/lo.1991.36.8.1662>, 1991.
- Mudie, P. J., Marret, F., Mertens, K. N., Shumilovskikh, L., and Leroy, S. A. G.: Atlas of modern dinoflagellate cyst distributions in the Black Sea Corridor: from Aegean to Aral Seas, including Marmara, Black, Azov and Caspian Seas, *Mar Micropaleontol*, 134, 1–152, <https://doi.org/10.1016/j.marmicro.2017.05.004>, 2017.
- Nooteboom, P. D., Bijl, P. K., Sebille, E., Heydt, A. S., and Dijkstra, H. A.: Transport Bias by Ocean Currents in Sedimentary Microplankton Assemblages: Implications for Paleooceanographic Reconstructions, *Paleoceanogr Paleoclimatology*, 34, 1178–1194, <https://doi.org/10.1029/2019pa003606>, 2019.

- Nooteboom, P. D., Delandmeter, P., Sebille, E. van, Bijl, P. K., Dijkstra, H. A., and Heydt, A. S. von der: Resolution dependency of sinking Lagrangian particles in ocean general circulation models, *Plos One*, 15, e0238650, <https://doi.org/10.1371/journal.pone.0238650>, 2020.
- 715 Nooteboom, P.D., Bijl, P.K., Kehl, C., Van Sebille, E., Ziegler, M., Von Der Heydt, A.S., Dijkstra, H.A.: Sedimentary microplankton distributions are shaped by oceanographically connected areas, *Earth System Dynamics*, 13 (1), pp. 357–371, DOI: 10.5194/esd-13-357-2022, 2022.
- Orsi, A. H., Whitworth, T., and Nowlin, W. D.: On the meridional extent and fronts of the Antarctic Circumpolar Current, *Deep Sea Res Part Oceanogr Res Pap*, 42, 641–673, [https://doi.org/10.1016/0967-0637\(95\)00021-w](https://doi.org/10.1016/0967-0637(95)00021-w), 1995.
- 720 Park, Y. H., Park, T., Kim, T. W., Lee, S. H., Hong, C. S., Lee, J. H., Rio, M. H., Pujol, M. I., Ballarotta, M., Durand, I., and Provost, C.: Observations of the Antarctic Circumpolar Current Over the Udintsev Fracture Zone, the Narrowest Choke Point in the Southern Ocean, *Journal of Geophysical Research: Oceans*, 124, 4511–4528, <https://doi.org/10.1029/2019JC015024>, 2019.
- Prebble, J.G., Crouch, E.M., Cortese, G., Carter, L., Neil, H., Bostock, H.: Southwest Pacific sea surface conditions during Marine Isotope Stage 11— Results from dinoflagellate cysts, *Palaeogeography, Palaeoclimatology, Palaeoecology*, 446, pp. 19–31, DOI: 10.1016/j.palaeo.2016.01.007, 2016.
- 725 Prebble, J. G., Crouch, E. M., Carter, L., Cortese, G., Bostock, H., and Neil, H.: An expanded modern dinoflagellate cyst dataset for the Southwest Pacific and Southern Hemisphere with environmental associations, *Mar Micropaleontol*, 101, 33–48, <https://doi.org/10.1016/j.marmicro.2013.04.004>, 2013.
- 730 Qin, X., Sebille, E. van, and Gupta, A. S.: Quantification of errors induced by temporal resolution on Lagrangian particles in an eddy-resolving model, *Ocean Model*, 76, 20–30, <https://doi.org/10.1016/j.ocemod.2014.02.002>, 2014.
- Rhodes, R. H., Bertler, N. A. N., Baker, J. A., Sneed, S. B., Oerter, H., and Arrigo, K. R.: Sea ice variability and primary productivity in the Ross Sea, Antarctica, from methylsulphonate snow record, *Geophys Res Lett*, 36, <https://doi.org/10.1029/2009gl037311>, 2009.
- 735 Sangiorgi, F., Bijl, P. K., Passchier, S., Salzmann, U., Schouten, S., McKay, R., Bohaty, S. M.: Southern Ocean warming and Wilkes Land ice sheet retreat during the mid-Miocene, *Nature communications*, 9(1), 317, 2018.
- Solodoch, A., Stewart, A. L., Hogg, A. M., Morrison, A. K., Kiss, A. E., Thompson, A. F., Purkey, S. G., and Cimoli, L.: How Does Antarctic Bottom Water Cross the Southern Ocean?, *Geophysical Research Letters*, 49, e2021GL097211, <https://doi.org/10.1029/2021GL097211>, 2022.
- 740 Spreen, G., Melsheimer, C., Malte Gerken, M. <https://seaice.uni-bremen.de/databrowser/> (last access: 17-12-2022). Institute of Environmental Physics, University of Bremen, Germany, 2015 – 2021
- Swalethorp, R., Dinasquet, J., Logares, R., Bertilsson, S., Kjellerup, S., Krabberød, A.K., Moksnes, P.-O., Nielsen, T.G., Riemann, L.: Microzooplankton distribution in the Amundsen Sea Polynya (Antarctica) during an extensive *Phaeocystis antarctica* bloom, *Progress in Oceanography*, Volume 170, Pages 1–10, <https://doi.org/10.1016/j.pocan.2018.10.008>, 2019.

- 745 Talley, L.: Closure of the Global Overturning Circulation Through the Indian, Pacific, and Southern Oceans: Schematics and Transports, *Oceanography*, 26, 80–97, <https://doi.org/10.5670/oceanog.2013.07>, 2013.
- Williams, G. L., Fensome, R. A., and MacRae, R. A.: The Lentin and Williams Index of Fossil Dinoflagellates, <https://doi.org/10.4095/103330>, 2017.
- Wilson, D. J., Bertram, R. A., Needham, E. F., van de Flierdt, T., Welsh, K. J., McKay, R. M., Mazumder, A., Riesselman, C.
- 750 R., Jimenez-Espejo, F. J., and Escutia, C.: Ice loss from the East Antarctic Ice Sheet during late Pleistocene interglacials, *Nature*, 561, 383–386, 10.1038/s41586-018-0501-8, 2018.
- Yool, A., Popova, E. E., and Anderson, T. R.: MEDUSA-2.0: an intermediate complexity biogeochemical model of the marine carbon cycle for climate change and ocean acidification studies, *Geosci Model Dev*, 6, 1767–1811, <https://doi.org/10.5194/gmd-6-1767-2013>, 2013.
- 755 Zonneveld, K. A. F., Marret, F., Versteegh, G. J. M., Bogus, K., Bonnet, S., Bouimetarhan, I., Crouch, E., Vernal, A. de, Elshanawany, R., Edwards, L., Esper, O., Forke, S., Grøsfjeld, K., Henry, M., Holzwarth, U., Kieft, J.-F., Kim, S.-Y., Ladouceur, S., Ledu, D., Chen, L., Limoges, A., Londeix, L., Lu, S.-H., Mahmoud, M. S., Marino, G., Matsouka, K., Matthiessen, J., Mildenhall, D. C., Mudie, P., Neil, H. L., Pospelova, V., Qi, Y., Radi, T., Richerol, T., Rochon, A., Sangiorgi, F., Solignac, S., Turon, J.-L., Verleye, T., Wang, Y., Wang, Z., and Young, M.: Atlas of modern dinoflagellate cyst distribution
- 760 based on 2405 data points, *Rev Palaeobot Palyno*, 191, 1–197, <https://doi.org/10.1016/j.revpalbo.2012.08.003>, 2013.

Supplementary Material

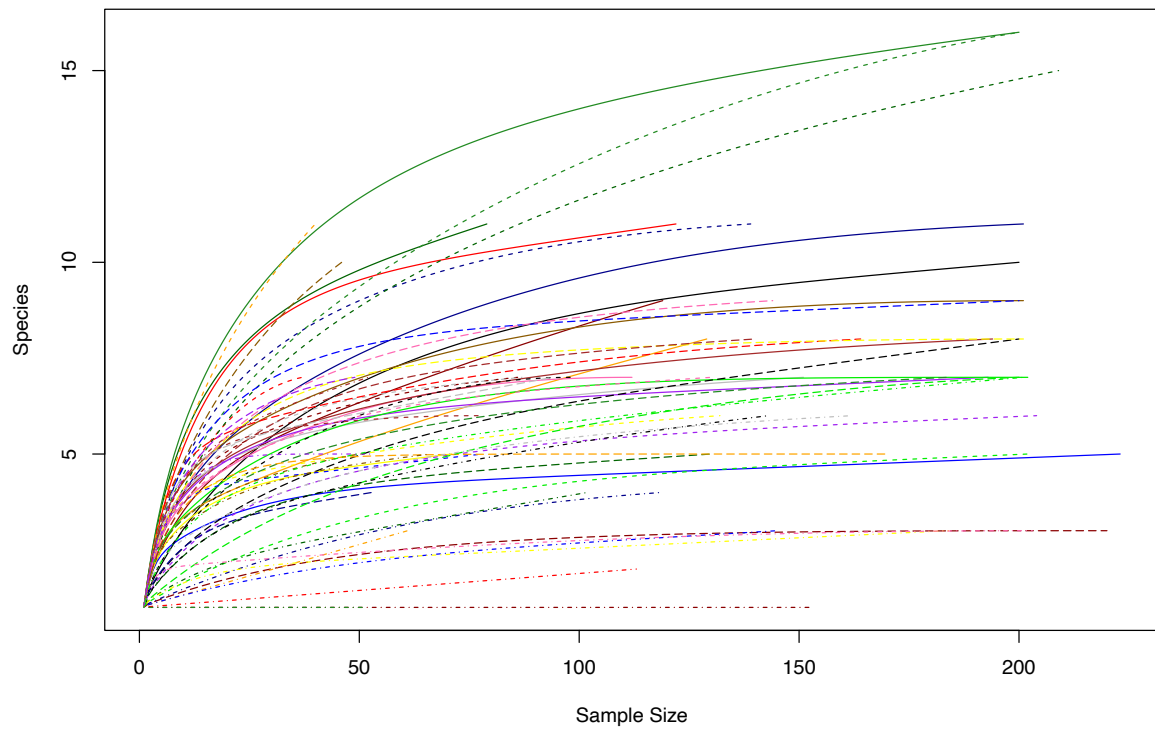


Figure S1. Rarefaction on dinocyst counts of the new samples.

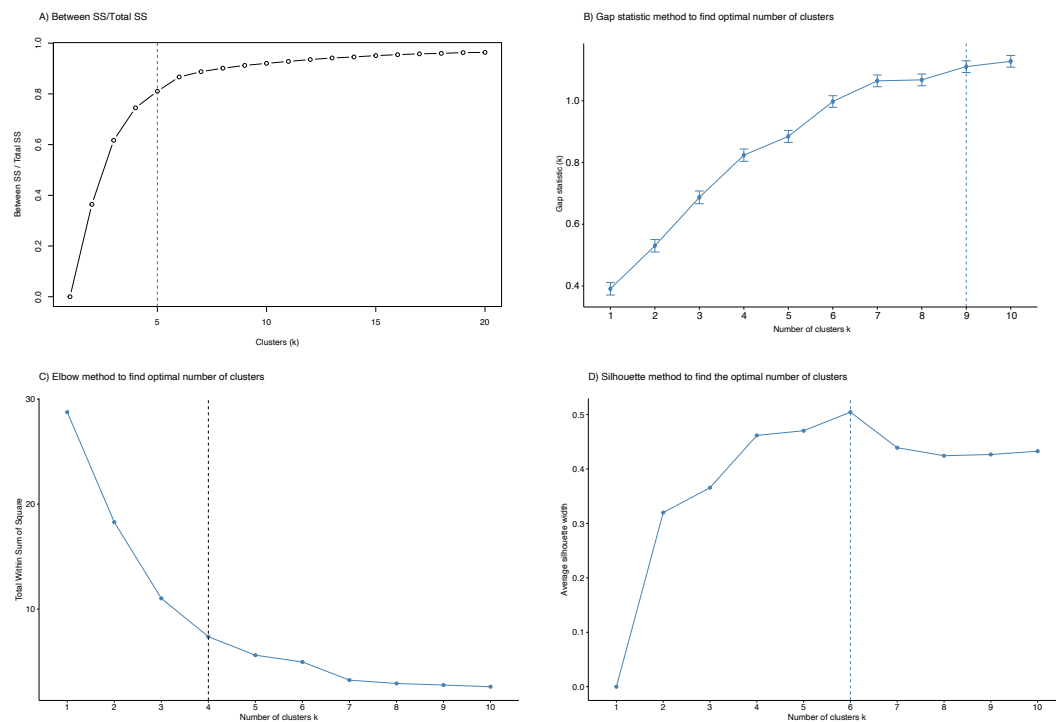


Fig. S2. Various methods to define the optimal clustering for dinocyst data in wsi_100.

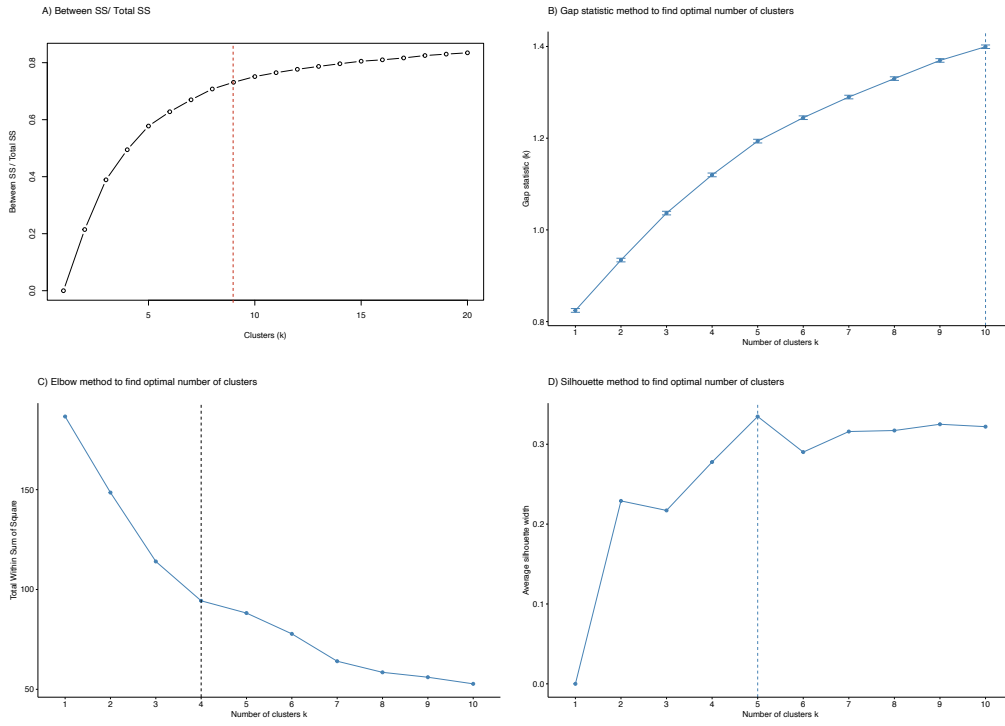


Fig. S3 Various methods to determine the optimal clustering of the dinocyst data in sh_655.